Dear Dr. Stef Lhermitte,

Thank you so much for the time and attention dedicated to this manuscript and for the valuable comments. Below, we answer point-by-point all the comments. The comments are reproduced in blue and the authors' responses (**AR**) are provided in black. The underlined texts are our corresponding changes in the revised manuscript. Pages (**P**) and lines (**L**) referred to in the response are directed to the revised manuscript with changes highlighted.

The main changes in the revised manuscript include:

- The robustness and the uncertainties of the DAV36$_{ice}$ algorithm were explained.
- The MEMLS simulations (including Figure 1) were removed.
- The area-averaged trend analyses were removed.
- A new section (3.2. Data preprocessing and analysis) was added.
- The comparison between snowmelt and climate indices was moved to the Methodology and Results Section.

Best regards,

Lei Zheng (on behalf of the co-authors)

Major remarks

1. I agree with R1 that Figure 1 does not directly conveys a clear message to your paper. I would recommend to either remove it (if Kang already showed that DAV is superior) or redesign (e.g. by showing a time series of single channel vs. DAV for different types of snowpacks) it such that it is clear that DAV method is superior. Currently, it is not very clear what the added value within the story is.

AR1: Figure 1 and the MEMLS simulations were removed. Instead, we cited the work which shows that DAV method is superior to the single-channel method:

Single-channel methods may fail to work when the Tb of a melting snowpack is even lower than the winter mean in the late melt season. By contrast, significant DAV variations still exist in the transition from a dry to wet snow regime during the heavy melt season. In addition, DAV is very sensitive to snowmelt and show very little variation in frozen seasons (Zheng et al., 2018). **(P5L20-24)**

2. Accuracy of the method: you indicate accuracies/Kappa-coefficients between Tair and satellite melt of 0.79 and 0.51 (for DAV) and 0.82 and 0.60 (for DAV_ice). Based on these values I doubt if these are strong enough to warrant any later interpretation of the trends (especially for the more chaotic EMO (see next point))? Please clarify this and take this uncertainty along if you later want to use the DAV signal for melt interpretations

AR2: The $DAV36_{ice}$ algorithm was utilized to detect melt signals on sea ice by mitigating the effect of open water. Actually, melt detection methods in polar regions have never been validated because of the absence of continuous and extensive snow wetness measurements. Tair can only provide evaluation rather than validation of the melt detection methods. The overall accuracy and Kappa coefficient between the positive Tair and satellite-detected melt signals were 0.82 and 0.60 (not 0.79 and 0.51), respectively.

The satellite-detected (25 km) and station-derived thaw/freeze state are not always strictly connected. For example, the overall accuracy between soil thaw/freeze status determined from satellite and ground temperature lies in the range of 0.79 to 0.92 (Jin et al., 2009; Zhao et al., 2011; Derksen et al., 2017; Kim et al., 2017). An overall accuracy of 0.82 between the thaw/freeze status estimated from microwave satellite and buoy Tair is acceptable. Moreover, a Kappa coefficient of 0.60 represents a fair to good strength of agreement (Fleiss et al., 2003). This is confirmed by the obtained p-value ($p < 0.05$). The mismatches largely occur in the period with transient snowmelt when thaw/freeze status shifted quickly and in the regions with plenty of open water (typical SIC < 90%). For the periods that were identified as thaw/freeze status for at least three days, satellite-derived melt signals showed close agreement (OA=0.87, Kappa=0.68) with that derived from Tair over the sea ice with SIC > 90%.

We explained the robustness of the $DAV36_{ice}$ algorithm in the revised manuscript:

> …while those were 0.82 and 0.60 based on the $DAV36_{ice}$ algorithm, indicating a fair to good strength of agreement according to Fleiss et al. (2003). (**P7L14-16**)
> The mismatches largely occur in the period with transient snowmelt when thaw/freeze status shifted quickly and in the regions with plenty of open water (typical SIC < 90%). For the periods that were identified as thaw/freeze status for at least three days, satellite-derived melt signals showed close agreement (OA=0.87, Kappa=0.68) with that derived from Tair over the sea ice with SIC > 90%. (**P7L19-22**)

We also explained and the reasons for the disagreements:

- First, the inconsistent temporal and spatial resolutions may result in disagreements in the period with transient melt events.

The disagreements in the identification of transient melt events may result from inconsistent spatial and temporal resolutions. Validating the large-scale satellite-based estimation (25 km for AMSR-E/2) against station-based measurements is always challenging due to representativeness errors (Lyu et al., 2017). The daily maximum Tair was derived from hourly Tair records, while only two daily satellite observations were used in the DAV method. (**P7L22-25**)

- Second, though the DAV36$_{ice}$ algorithm can mitigate the effect of open water, we acknowledge that melt detection over the sea ice is still challenging because of the ice disintegrates, brine and flooding. We have clarified this issue:

  In the marginal sea ice zone, ice disintegrates, brine and flooding effects may play an important role in seasonal and even diurnal sea ice Tb variations, further complicating the story (Smith, 1998; Willmes et al., 2009). (**P7L25-27**)

In view of this, we removed the trend analysis of EMO in the revised manuscript:

  EMO is not included in the trend analysis because of the chaotic spatial distribution of the early transient melt events. (**P10L31-32**)

3. I agree with R1 that the early melt onset seems very much random early effect with little physical meaning and/or impact. Therefore, I wonder if the regression on these time series have any physical meaning? I would definitely consider removing the trend analysis of the EMO

AR3: We thank the editor for the suggestion. The trend analysis of the EMO was removed.

4. You only introduce the trend regression in the results (which should already be done in the methods) and it is completely unclear how the trends (already indicated by R1) were observed and where their uncertainty comes from. Is it on a per-pixel basis and afterwards spatially merged (and how?) or first spatial merging and then trend-analyses? How were the uncertainties calculated, etc?

AR4: Trends at every pixel with continuous records were firstly calculated, and the area-averaged trends were afterwards spatially merged. The trends were reported in days per year, with uncertainties determined using the degrees of freedom present in the regression residuals at the 90% confidence level.

We introduced how the trends were calculated in the Methodology Section:

  Linear trends were calculated using a least-squares adjustment (**P9L7-8**)

The area-averaged trend analyses were removed according to the editor's suggestion in the next comment (please see **AR5** for full details).

5. I have my severe doubts about the physical meaning of the trends (especially for the EMO, which seems very stochastic (as also indicated by R1)). I would reconsider removing all trend analyses from the paper and or add more clarity on the methods (how did you do the patio-temporal averaging?)

AR5: The area-averaged trend analyses (including Table 2 and Fig. 8) were removed in the revised manuscript, but we would like to keep the trend analyses at pixel-scale (excluding EMO) which can show the localized changes in snowmelt timing. We explained how the trend and significance level were calculated in Section 3.2 (Data preprocessing and analysis):

> Linear trends were calculated using a least-squares adjustment. The significance levels of the correlations and regressions were determined using the Student's t-tests. (**P9L7-9**)

6. The comparison with the atmospheric indices should already be introduced in the results/methods sections and not left until the discussion.

AR6: We thank the editor for the suggestion. The comparison was moved to the Methodology Section and Results Section. Additionally, we explained how climate indices were calculated:

> To study the response of the pan-Antarctic surface snowmelt to circulation conditions, we explored the relationship between the melt indices and El Niño/Southern Oscillation (ENSO) and Southern Annular Mode (SAM). Nino3.4, the average sea surface temperature anomaly in the tropical (170°W–120°W, 5°S–5°N), is calculated from the Hadley Centre Sea Ice and Sea Surface Temperature dataset (Rayner et al., 2003). Southern Oscillation Index (SOI) is calculated using the pressure difference between Tahiti and Darwin (Ropelewski et al., 1987). Southern Annular Mode is calculated using the zonal pressure difference between 40°S and 65°S (Marshall, 2003). (**P9L10-15**)

PDF Comments

7. P1L21-22. Given the large intermittent character of EMO, I would remove your trend analyses from the paper.

AR7: Trend analysis of EMO was removed as suggested.

8. P3L11-12. Based on the sentence I derive that the units of these values are time, but I really have difficulty the numbers here as time. Please use hour+minutes (or seconds) as unit and modify the values accordingly.

AR8: The values were changed to hour±minutes：

> …the local acquisition time of ascending and descending SSM/I Tb products south of 40° S were 19:10±26 minutes and 5:27±27 minutes, respectively, while these values were 14:09±12 minutes and 0:53±12 minutes for the AMSR-E Tb products. (**P3L11-13**)

9. P4L14-15. Delete "University of Colorado Boulder".

AR9: Done.

10. P4L15. I guess that you mean over the data whole period and that this is a way to remove all ice free zones. If so, please indicate that it is over the whole period.

AR10: Yes. We clarified this issue:

> To remove ice-free zones over the whole period, pixels with SIC greater than 80% for less than 5 days were not included in the analyses (Markus et al., 2009). (**P4L17-18**)

11. P4L22. What resampling scheme was used? Nearest neightbor, linear, ...

AR11: Nearest-neighbor interpolation was used. We clarified this issue:

> … and resampled to the same spatial resolution as the passive microwave measurements (25 km) using nearest-neighbor interpolation. (**P4L25-26**)

AR12: The $DAV36_{ice}$ algorithm was utilized in melt detection over sea ice rather than the DAV algorithm. The overall accuracy and Kappa coefficient between the positive maximum Tair and satellite-detected melt signals based on the $DAV36_{ice}$ algorithm used in this study were 0.82 and 0.60 respectively.

The satellite-detected (25 km) and station-derived thaw/freeze state are not always strictly connected. For example, the overall accuracy between soil thaw/freeze status determined from satellite and ground temperature lies in the range of 0.79 to 0.92 (Jin et al., 2009; Zhao et al., 2011; Derksen et al., 2017; Kim et al., 2017). An overall accuracy of 0.82 between the thaw/freeze status estimated from microwave satellite and buoy Tair is acceptable. Moreover, a Kappa coefficient of 0.60 represents a fair to good strength of agreement (Fleiss et al., 2003). This is confirmed by the obtained p-value ($p < 0.05$). The mismatches largely occur in the period with transient snowmelt when thaw/freeze status shifted quickly and in the regions with plenty of open water (typical SIC < 90%). For the periods that were identified as thaw/freeze status for at least three days, satellite-derived melt signals showed close agreement (OA=0.87, Kappa=0.68) with that derived from Tair over the sea ice with SIC > 90%.

We explained the robustness of the $DAV36_{ice}$ algorithm in the revised manuscript:

> …while those were 0.82 and 0.60 based on the $DAV36_{ice}$ algorithm, indicating a fair to good strength of agreement according to Fleiss et al. (2003). (**P7L14-16**)
> The mismatches largely occur in the period with transient snowmelt when thaw/freeze status shifted quickly and in the regions with plenty of open water (typical SIC < 90%). For the periods that were identified as thaw/freeze status for at least three days, satellite-derived melt signals showed close agreement (OA=0.87, Kappa=0.68) with that derived from Tair over the sea ice with SIC > 90%. (**P7L19-22**)

We also explained and the reasons for the disagreements:

- First, the inconsistent temporal and spatial resolutions may result in disagreements in the period with transient melt events.
  The disagreements in the identification of transient melt events may result from inconsistent spatial and temporal resolutions. Validating the large-scale satellite-based estimation (25 km for AMSR-E/2) against station-based measurements is always challenging due to representativeness errors (Lyu et al., 2017). The daily maximum Tair was derived from hourly Tair records, while only two daily satellite observations were used in the DAV method. (**P7L22-25**)

- Second, though the DAV36$_{ice}$ algorithm can mitigate the effect of open water, we acknowledge that melt detection over the sea ice is still challenging because of the ice disintegrates, brine and flooding. We have clarified this issue:

  In the marginal sea ice zone, ice disintegrates, brine and flooding effects may play an important role in seasonal and even diurnal sea ice Tb variations, further complicating the story (Smith, 1998; Willmes et al., 2009). (**P7L25-27**)
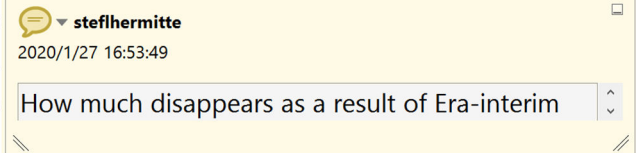
In view of this, we removed the trend analysis of EMO in the revised manuscript:

  EMO is not included in the trend analysis because of the chaotic spatial distribution of the early transient melt events. (**P10L31-32**)

13. P7L6. "complete melt seasons". How much disappears as a result of Era-interim?

AR13: We are so sorry that we fail to catch what the editor means here. We would appreciate it if the editor could elaborate more on this comment.

To capture complete melt seasons, a melting year begins on 1 July and ends on 30 June of the next year. The missing observations were filled based on tin | signals, which can be caused by cloud | errors. To mitigate their impacts on me | Further, melt detection was constraine

steflhermitte
2020/1/27 16:53:49

How much disappears as a result of Era-interim

mistaken for melt | residual calibration | tellite observations. | y et al. (2004). The

14. P7L9. "median filter". Spatial? Perhaps add spatial to clearly indicate it is a spatial filter?

AR14: We clarified this issue:

  To mitigate their impacts on melt detection, a median **spatial** filter with a 3×3 window was applied to the satellite observations. (**P9L5**)

15. P7L14. "was" → "were".

AR15: Done.

16. P7L16. "disappears". You mean: when it drops below 15% SIC?

AR16: Yes, we revised this sentence to clarify:

> In such cases, the last day of snowmelt is always the day that SIC drops below 15%, rather than the day that freeze-up begins. (**P8L12-14**)

17. P8L3. "parts" → "sub-areas"?

AR17: Done.

18. P8L6. "AIS" → "including all Antarctic ice shelves".

AR18: We revised this sentence to clarify:

> … and the AIS including all floating ice shelves. (**P9L21**)

19. P8L22. Add "...from AMSR-E/2 satellite observations and ERA-reanalyses agreed well...".

AR19: Done.

20. P8L23. Is that well? They are often outside each other confidence limits, so I definitely don't agree with 'well'. What is the impact here and how reliable are your results in that 'not that well' context?.

AR20: We agree that snowmelt timing derived from the two methods show local discrepancies, especially in the marginal sea ice zone. We revised this sentence:

> Melting timing derived from AMSR-E/2 satellite observations and ERA-Interim reanalyses generally agreed well with each other in the AIS and IO, but showed some discrepancies in other regions (Table 1 and Fig. 4). (**P10L6-7**)

We are sorry to make it confusing here. The same as Markus et al. (2009), we compared the snowmelt from reanalysis Tair and the satellite observations to show that they have similar spatial distribution patterns, rather than to validate the satellite estimations. We clarified this issue in the revised manuscript:

> Melt timing derived from different approaches are supposed to show similar spatial distribution patterns. To evaluate the performance of the DAV method on a larger scale, snowmelt over the pan-Antarctic was also determined by ERA-Interim reanalysis when the daily maximum Tair exceeded -1°C. (**P7L30 & P8L1-2**)

Similar discrepancies between the results from the reanalysis and satellite were also found in the Arctic (Markus et al., 2009):
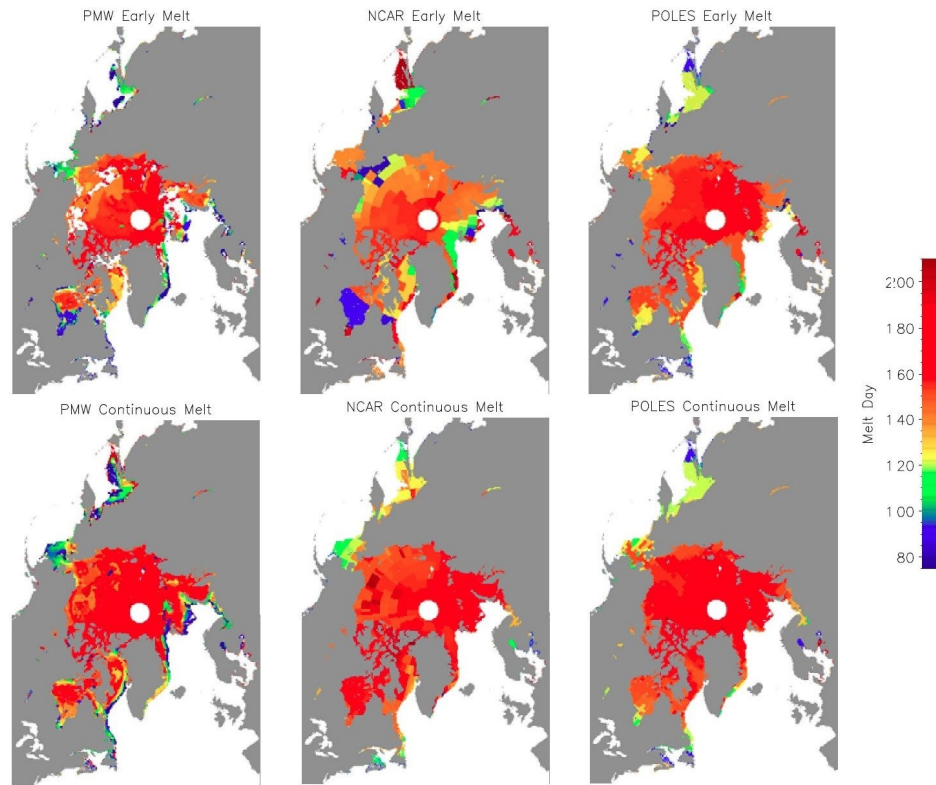

Figure R1. Examples of melt onset for 2004 from passive microwave (PMW) data and from the NCEP/NCAR and POLES data sets. NCAR and POLES melt data are determined by a threshold in temperature of -1℃. Temperatures above this threshold indicate melt conditions. For the POLES data we distinguish between earliest melt and continuous melt. "Earliest melt" indicates the day when temperatures go above the threshold temperature for the first time while "continuous melt" indicates the day when temperatures remain above the threshold temperature for the summer (figure revised from Markus et al. (2009)).

This is mainly because Tair above/below the freezing point does not always indicate a melting/frozen snowpack. Markus et al. (2009) showed that varying the threshold applied to Tair by ±2℃ can result in a range of ±50 days for melt timing. In addition, it takes time to produce meltwater when melt energy is available. We explained the reasons for the disagreements in the revised manuscript:

Tair above/below the freezing point does not always indicate a melting/frozen snowpack. EMO and CMO derived from ERA-Interim were earlier than that detected by AMSR-E/2 data (Fig. 4 and Table 1). This is because it takes time to produce liquid water when snow temperature approaches the melting point. Daily Tb variation is limited when liquid water does not refreeze or snowpack is still melting in the warm nights during heavy melt seasons (Willmes et al., 2009;

Semmens and Ramage, 2014). As a result, ERA-Interim recognized more melt events for the regions where heavy snowmelt was found and the DAV method fails to work, such as the WS, BAS, RS and the Larsen C ice shelf. This might also be the reason that the melt onset was very early in RS while few melt events were detected by AMSR-E/2. (**P12L17-23**)

21. P9L1. "Approximately16%". Space missing.

AR21: Corrected.

22. P9L11. This trend analyses should be introduced already in the method section and it should be definitely be indicated how this was done (how did you spatially combine the pixels, what do you do with the uncertainties, etc). Did you first calculate the regional mean and subsequently applied regression on the time series of means and/or did calculate the trends per pixel and subsequently merged them? Etc..

AR22: Trends at every pixel with continuous records were firstly estimated, and the area-averaged trends were afterwards spatially merged. The trends were reported in days per year, with uncertainties determined using the degrees of freedom present in the regression residuals at the 90% confidence level.

We introduced how the trends were calculated in the Methodology Section:

> Linear trends were calculated using a least-squares adjustment (**P9L7-8**)

The area-averaged trend analyses were removed according to the editor's suggestion (please see **AR5** for full details).

.

23. P9L20. "Fig. 8". Add titles/labels + uncertainties.

AR23: The area-averaged trend analyses (including Fig. 8) were removed as suggested.

24. P9L20. "much later". Is it?.

AR24: Yes, EMO over the period 2013-2017 was on average about 12 days later compared with that in 2011/2012.

25. P10L26. Or you may overestimate? I don't see any hard proof that any method is better than the other and you should allow more interpretation of whom is better.

AR25: Yes, we cannot tell which method is more accurate given that we did not directly validate the methods and the results from ERA-Interim can only serve as a reference.

We revised this part with more interpretation of the strength and weakness of the two methods:

> AMSR-E/2 and ERA-Interim daily mean melt extent were more than twice the melt extent mapped by PF06 from December to February (Fig. 10b). In a recent study, PF06 melt extent was also found to be much smaller compared with that derived from scatterometers (Zheng et al., 2020). PF06 determined snowmelt when the SSM/I 19 GHz Tb exceeds the winter mean plus 2.5 times the standard deviation of the winter Tb. During the melt seasons, Tb may decrease due to the strong volume scattering resulting from the increase of snow grain size and the formation of icy layers (Ramage and Isacks, 2002; Markus et al., 2009). Summer Tb can even be much lower than the winter observations (Zheng et al., 2018). Therefore, PF06 may underestimate surface snowmelt when snow metamorphism occurs in melt season. The DAV method is unaffected by snow metamorphism but may fail to work when liquid water does not refreeze or snowpack is still melting in warm nights (Willmes et al., 2009). Fortunately, the Antarctic surface snowmelt is always short-lived and can refreeze quasi-instantaneously (Zheng et al., 2018; van den Broeke et al., 2010a). (**P13L5-14**)

26. P11L17. "Response of the pan-Antarctic surface snowmelt to atmospheric indices". Should be a result, not a discussion.

AR26: This section was moved to Results.

27. P12L16. "positive Tair observations", of what type of observations?.

AR27: Good catch. We revised this sentence to clarify:

> …snowmelt detected by AMSR-E/2 agreed well with the **in-situ** positive Tair observations, and was more extensive than that detected by SSM/I. (**P15L9-10**)

28. P12L18. Avoid abbreviations in the conclusions, so also people that want to have a quick look, can

AR28: Abbreviations were changed to full names in the Conclusions.

29. P12L23-26. I agree, but I think this should also be addressed in the discussion and not left for the conclusion.

AR29: This part was moved to Section 5.2 (Uncertainties).

References:

Markus, T., Stroeve, J. C. and Miller, J.: Recent changes in Arctic sea ice melt onset, freezeup, and melt season length, J. Geophys. Res., 114, C12024, doi:10.1029/2009JC005436, 2009.

Marshall, G. J.: Trends in the Southern Annular Mode from observations and reanalyses, J. Clim., 16(24), 4134–4143, doi:10.1175/1520-0442(2003)016<4134:TITSAM>2.0.CO;2, 2003.

Rayner, N. A., Parker, D. E., Horton, E. B., Folland, C. K., Alexander, L. V., Rowell, D. P., Kent, E. C. and Kaplan, A.: Global analyses of sea surface temperature, sea ice, and night marine air temperature since the late nineteenth century, J. Geophys. Res., 108(D14), 4407, doi:10.1029/2002JD002670, 2003.

Ropelewski, C. F. and Jones, P. D.: An Extension of the Tahiti–Darwin Southern Oscillation Index, Mon. Weather Rev., 115(9), 2161–2165, doi:10.1175/1520-0493(1987)115<2161:AEOTTS>2.0.CO;2, 1987.

Semmens, K. and Ramage, J.: Melt patterns and dynamics in Alaska and Patagonia derived from passive microwave brightness temperatures., Remote Sens., 6(1), 603–620, doi:10.3390/rs6010603, 2014.

Willmes, S., Haas, C., Nicolaus, M. and Bareiss, J.: Satellite microwave observations of the interannual variability of snowmelt on sea ice in the Southern Ocean, J. Geophys. Res. Ocean., 114(3), 1–13, doi:10.1029/2008JC004919, 2009a.

Willmes, S., Haas, C., Nicolaus, M. and Bareiss, J.: Satellite microwave observations of the interannual variability of snowmelt on sea ice in the Southern Ocean, J. Geophys. Res., 114, C03006, doi:10.1029/2008JC004919, 2009b.

Zheng, L., Zhou, C., Liu, R. and Sun, Q.: Antarctic Snowmelt Detected by Diurnal Variations of AMSR-E Brightness Temperature, Remote Sens., 10(9), 1391, doi:10.3390/rs10091391, 2018.

Zheng, L., Zhou, C. and Liang, Q.: Variations in Antarctic Peninsula snow liquid water during 1999–2017 revealed by merging radiometer, scatterometer and model estimations, Remote Sens. Environ., 232, 111219, doi:10.1016/j.rse.2019.111219, 2019.

Zheng, L., Zhou, C. and Wang, K.: Enhanced winter snowmelt in the Antarctic Peninsula : Automatic snowmelt identi fi cation from radar scatterometer, Remote Sens. Environ., 246, 111835, doi:10.1016/j.rse.2020.111835, 2020.

Recent changes in pan-Antarctic surface snowmelt detected by AMSR-E and AMSR2

Lei Zheng[1], Chunxia Zhou[1], Tingjun Zhang[2], Qi Liang[1], Kang Wang[3]

[1]Chinese Antarctic Center of Surveying and Mapping, Wuhan University, Wuhan 430079, China
[2]Key Laboratory of Western China's Environmental Systems (Ministry of Education), College of Earth and Environmental Sciences, Lanzhou University, Lanzhou 730000, China
[3]Institute of Arctic and Alpine Research, University of Colorado Boulder, Boulder, Colorado, 80309, USA

Correspondence to: Chunxia Zhou (zhoucx@whu.edu.cn) and Tingjun Zhang (tjzhang@lzu.edu.cn)

Abstract. Surface snowmelt in the pan-Antarctic, including the Antarctic ice sheet (AIS) and sea ice, is crucial to the mass and energy balance in polar regions and can serve as an indicator of climate change. Here, we investigated the spatial and temporal variations in the surface snowmelt over the entire pan-Antarctic from 2002 to 2017 by using the passive microwave remote sensing data. The stable orbit and appropriate acquisition time of the Advanced Microwave Scanning Radiometer for the Earth Observing System (AMSR-E) and the Advanced Microwave Scanning Radiometer 2 (AMSR2) enable us to take full advantage of the daily brightness temperature (Tb) variations to detect the surface snowmelt. In this study, the difference between AMSR-E/2 ascending and descending 36.5 GHz Tb in vertical polarization (DAV36) was utilized to map the pan-Antarctic snowmelt because it is unaffected by the snow metamorphism. We evaluated the DAV36 algorithm against ground-based measurements and further improved the method over the marginal sea ice zone by excluding the effect of open water. Snowmelt detected by AMSR-E/2 data was more extensive and persistent than that detected by the Special Sensor Microwave/Imager (SSM/I) data. On average, pan-Antarctic early snowmelt onset (EMO) occurs in late September, while continuous melt onset (CMO) occurs in mid-November. ~~Overall, pan-Antarctic surface snowmelt showed a trend (at the 90% confidence level) towards later EMO (0.68 days yr⁻¹) during the 2002-2017 period.~~ Pan-Antarctic CMO was significantly correlated (at the 95% confidence level) with summer Southern Annular Mode (SAM). The decreased surface snowmelt on the AIS was very likely linked with the enhanced summer SAM.

1 Introduction

Surface snowmelt on sea ice and ice sheets has a great influence on the energy exchange between the snow surface and atmosphere because wet snow has a lower albedo, and thus absorbs more incoming solar radiation than dry snow (Steffen, 1995). Intense snowmelt leads to the formation of melt ponds on sea ice and ice sheets, which in turn absorb more radiation and induce further snowmelt through melt-albedo feedback (Tanaka et al., 2016; Bell et al., 2018). Meltwater may fill in the ice crevasses on ice sheets and migrate to the ice-bedrock surface, which can induce the acceleration of ice flow (Zwally et al.,

2002; Sundal et al., 2011). Meltwater can also transport heat into crevasses and deepen them, providing the conditions for ice shelves to break up through hydrofracturing (Scambos et al., 2000; van den Broeke, 2005). Therefore, the spatial and temporal dynamics of surface snowmelt on sea ice and ice sheets have a direct effect on mass and energy balances in polar regions (Picard and Fily, 2006; van den Broeke et al., 2009; Stroeve et al., 2014). The timing and extent of surface snowmelt are

5   indicators of changes in polar climate (Intergovernmental Panel on Climate Change (IPCC), 2014), and thus potentially have regional and global climate implications.

In-situ observations of snowmelt are sparse over sea ice and ice sheets due to an unfavorable environment. Remote sensing techniques can provide timely data sets for the monitoring of melt events in polar regions. When a snowpack begins to melt, the most significant change in the electromagnetic properties is an abrupt increase in the dielectric constant, which increases

10   absorption and reduces the penetration depth of microwaves (Ashcraft and Long, 2006). Therefore, snowmelt can be detected via microwave radiometry by identifying the sharp changes in microwave brightness temperatures (Tb) caused by the presence of snow liquid water (Serreze et al., 1993; Liu et al., 2005).

Microwave radiometers can operate regardless of illumination conditions and are insensitive to atmospheric conditions. Most spaceborne passive microwave instruments provide more than two daily passes in polar regions. Scanning Multi-channel

15   Microwave Radiometer (SMMR) 18 GHz and 37 GHz Tb and Special Sensor Microwave/Imager (SSM/I) 19 GHz and 37 GHz Tb have been used to detect surface snowmelt on ice sheets when Tb is above a region-specific or user-defined constant depending on the local snow properties (Ridley, 1993; Zwally and Fiegles, 1994; Mote and Anderson, 1995; Tedesco, 2009). Tb received by satellites is also related to the ground physical temperature, clouds and atmospheric water vapor, which may contaminate melt signals in the Tb time series. Multi-channel methods were developed to minimize these interferences, e.g.,

20   using a gradient ratio or a cross-polarized gradient ratio (XGPR) between 19 GHz and 37 GHz to detect surface snowmelt on sea ice and ice sheets (Abdalati and Steffen, 1995; Markus et al., 2009; Liang et al., 2013; Arndt et al., 2016). Snowmelt can also be recognized based on edge detection or wavelet transform-based technologies by identifying the abrupt changes in Tb values (Joshi et al., 2001; Liu et al., 2005).

Snow grain size increases after the liquid water refreezes. As a result, dry snow Tb decreases during the melt season due to

25   the increase in volume scattering (Markus et al., 2009). Therefore, single-channel methods may fail to identify melt events because of the metamorphic snow structures. Ramage and Isacks (2002, 2003) introduced the SSM/I diurnal amplitude variations (DAV, i.e., the Tb difference between ascending and descending passes) in vertically polarized 37 GHz Tb to investigate the snowmelt timing on the Southeast Alaskan Icefields. The DAV method is unaffected by snow metamorphism in melt detection. This technique has been successfully applied to ice sheets and was proven to be more sensitive to snow

30   liquid water than the XGPR method (Tedesco, 2007; Zheng et al., 2018). Freeze-thaw cycles on the Antarctic sea ice were also successfully detected based on the SSM/I 37 GHz DAV (Willmes et al., 2009). Furthermore, Arndt et al. (2016) distinguished temporary snowmelt from continuous snowmelt on the Antarctic sea ice by combining DAV with the cross-polarized ratio of SSM/I Tb. In these studies, surface snowmelt patterns were not described over the marginal sea ice zone, where the earliest

sea ice retreat was identified (Stammerjohn et al., 2008). DAV may not be strong enough to be identified as melt signals when open water with low Tb emerges in the first-year sea ice zone.

Most of these studies investigated surface snowmelt on sea ice and ice sheets based on SSM/I sensors. However, SSM/I observations show considerable variations in local acquisition time because of orbit degradation (Picard and Fily, 2006). By contrast, the Advanced Microwave Scanning Radiometer for the Earth Observing System (AMSR-E) and the Advanced Microwave Scanning Radiometer 2 (AMSR2) operate in controlled-orbits so that local acquisition time shows little temporal variation (http://www.remss.com/support/crossing-times). AMSR-E/2 measurements with a stable orbit are superior in the analyses of inter-annual snowmelt dynamics. Diurnal melt area in the Antarctic varies approximately as a sinusoid with the peak in the afternoon and the trough in the early morning (Picard and Fily, 2006). AMSR-E/2 can monitor the Antarctic sea ice and ice sheet (referred to as pan-Antarctic) surface snowmelt at the appropriate local acquisition time. Taking 2002-2003 as an example, the local acquisition time of ascending and descending SSM/I Tb products south of 40° S were 19:10±26 minutes and 5:27±27 minutes~~19.17±0.44 and 5.45±0.45~~, respectively, while these values were 14:09±12 minutes and 0:53±12 minutes~~14.16±0.20 and 0.88±0.20~~ for the AMSR-E Tb products. Compared with SSM/I, AMSR-E/2 have more opportunities to detect melt events in the pan-Antarctic due to warmer and colder periods for ascending and descending passes and an expected higher DAV.

Unlike the Arctic sea ice and Greenland ice sheet, pan-Antarctic surface snowmelt is relatively short-lived and patchy (Drinkwater and Liu, 2000; Picard et al., 2007), and has received much less attention. Contrary to the reduction in sea ice extent, thickness and duration in the Arctic, the Antarctic sea ice presented increasing trends in both extent and duration, especially in the Ross Sea (Comiso and Nishio, 2008; Hobbs et al., 2016). Most of the Antarctic sea ice is snow-covered, even in summer when snowmelt occurs (Brandt et al., 2005). Melt ponds are not often observed on the Antarctic sea ice (Ackley et al., 2008). Meltwater on the Antarctic ice sheet (AIS) can refreeze quasi-instantaneously (van den Broeke et al., 2010a) and contributes little to the surface mass balance (The IMBIE team, 2018). Although more than 25% of the AIS has experienced snowmelt since the 1980s, only 2% melts every year (Picard et al., 2007). Melt extent has been decreasing over the AIS since 1987 (Tedesco et al., 2007).

Strong interactions have been found between sea ice and ice sheet surface snowmelt through atmospheric circulation (Stroeve et al., 2017). Surface snowmelt dynamics in the West Antarctic and Antarctic peninsula have been found to be related with the sea ice variations in adjacent seas (Scott et al., 2018; Zheng et al., 2019). Previous studies have separately investigated surface snowmelt on sea ice and ice sheet, which may result in uncertainties in the integrated study. The DAV method has been successfully applied in snowmelt detection on both sea ice (Willmes et al., 2009) and ice sheet (Tedesco, 2007; Zheng et al., 2018). It is worthwhile to estimate snowmelt over the pan-Antarctic based on a uniform approach. The overall objective of this study is to improve the understanding of surface snowmelt over the pan-Antarctic based on the DAV method in three aspects: (1) to detect the pan-Antarctic surface snowmelt at the stable and appropriate local acquisition time based on AMSR-E/2, (2) to improve the performance of the DAV method in the marginal sea ice zone by excluding the effect of open water,

and (3) to estimate the pan-Antarctic surface snowmelt as a whole and systematically describe the surface snowmelt patterns and changes from 2002 to 2017.

2 Data sets

2.1 Data from AMSR-E/2

5 A modified version of the AMSR radiometer, the AMSR-E radiometer, launched aboard the NASA Earth Observing System (EOS) Aqua satellite on 4 May 2002. We obtained the 25 km AMSR-E/Aqua L2A global swath spatially-resampled 36 GHz Tb data from the National Snow and Ice Data Center (NSIDC, www.nsidc.org) (Knowles et al., 2006). AMSR2 aboard the Global Change Observation Mission-Water (GCOM-W1) satellite was launched on 18 May 2012 after AMSR-E ceased operations. As a successor of AMSR-E, AMSR2 shares almost the same satellite orbit and sensor parameters as AMSR-E, and

10 provides continuous measurements for the study of global climate change, energy balance and ecosystems. The 25 km AMSR2 Tb used in this study was provided by the Japan Aerospace Exploration Agency (JAXA, http://suzaku.eorc.jaxa.jp/GCOM/). AMSR-E/2 obtained data over a 1450 km swath. The brightness temperature products at 36.5 GHz in vertical polarization (Tb_{V36}) was used to estimate the pan-Antarctic snowmelt extent and timing in this study.

2.2 Sea ice and atmospheric products

15 The Bootstrap sea ice concentration (SIC) product was used to mask sea ice in this study (Comiso, 2017). The 25 km daily SIC South Hemisphere product was obtained from the NSIDC (http://nsidc.org/data/nsidc-0079), University of Colorado Boulder. To remove ice-free zones over the whole period, Ppixels with SIC greater than 80% for less than 5 days were not included in the analysesmarked as being ice free (Markus et al., 2009). For a sea ice pixel, SIC above 15% indicates the presence of sea ice (Meier and Stroeve, 2008).

20 ERA-Interim is a global reanalysis produced by the European Centre for Medium-Range Weather Forecasts (ECMWF). The ERA-Interim reanalysis includes various surface parameters, describing weather, ocean and land-surface conditions since 1979 (Dee et al., 2011). The 6-hourly air temperature (Tair) from the gridded ERA-Interim reanalysis at 2 m height was used to assist with melt detection based on AMSR-E/2, as well as directly determine snowmelt in this study.

The sea ice product is provided in the NSIDC EASE-Grid projection, which is the same as the AMSR-E/2 products. The

25 0.5° gridded ERA-Interim reanalysis was reprojected to the NSIDC EASE-Grid, and resampled to the same spatial resolution as the passive microwave measurements (25 km) using nearest-neighbor interpolation.

3 Methodology

3.1 Melt detection method Tb and liquid water content

According to the Rayleigh-Jeans approximation, Tb is a function of emissivity (ε) and the near-surface physical temperature (Ts) of snow and ice (Zwally, 1977):

$$Tb = \varepsilon Ts \tag{1}$$

Previous studies have emphasized the process that Tb increases when the snowpack starts to melt due to the increase in emissivity. However, Tb decreases after reaching a peak when the volumetric volume liquid water is approximately about one percent (Kang et al., 2014). We investigated the variations in Tb_{V36} with increasing snow liquid water based on the Microwave Emission Model of Multi-layered Snowpack (MEMLS) (Wiesmann and Mätzler, 1999). In the simulations, snow temperature, density and depth in a homogeneous snowpack were set to 273.15 K, 350 kg m⁻³, and 20 cm, respectively, by referring to Brucker et al. (2010) and Kang et al. (2014). Snow-ice reflectivity at 36.5 GHz was set to 0.045 in vertical polarization according to Powell et al. (2006). The evolution of Tb with increasing liquid water can be divided into energy saturation and energy dampening phases. The initial increases in Tb are accompanied by the amplification of ε until the liquid water reaches a certain level. The subsequent energy dampening phase is characterized by monotonic decreases in Tb, which are caused by the increase in snow-air interface reflectivity due to the amplified real part of the refractive index (Kang et al., 2014) (Fig. 1). Tb_{V36} of the fine-grained snowpack increases rapidly in the energy saturation phase with a slight amount of liquid water, and daily Tb variations are large because of the contrasting freeze/thaw state. Therefore, both single-channel and DAV methods can recognize these sharp changes in the early melt season. During the melt seasons, snow grain size can increase to 2 mm when meltwater refreezes in the pore space (Winebrenner et al., 1994). As a result, Tb_{V36} of the coarse-grained snowpack is much lower than that of the fine-grained snowpack due to enhanced volume scattering. Single-channel methods may fail to work when the Tb_{V36} of a melting snowpack is even lower than the winter mean in the late melt season (Zheng et al., 2018). By contrast, significant daily Tb_{V36} DAV variations still exist in the transition from a dry to wet snow regime during the heavy melt season. In addition, DAV is very sensitive to snowmelt and show very little variation in frozen seasons (Zheng et al., 2018). even when day-time Tb_{V36} is in the energy dampening phase (Zheng et al., 2018) (Fig. 1). Diurnal freeze-thaw cycles are prevalent in polar regions (Hall et al., 2009; Willmes et al., 2009; van den Broeke et al., 2010b). The simulations suggest that the DAV method can detect melt signals for both the melt onset (e.g., Willmes et al., 2009) and the entire melt season when diurnal freeze/thaw transition occurs (e.g., Zheng et al., 2018). Moreover, the optimum acquisition time of AMSR-E/2 enables us to take full advantage of the DAV method in melt detection.

3.2 Melt detection methods

A vertically polarized SSM/I 37 GHz DAV (DAV37) has been used in melt detection on the Greenland ice sheet and Antarctic sea ice (Willmes et al., 2006, 2009; Tedesco, 2007; Arndt et al., 2016). Extensive summer daily freeze-thaw cycles on the Antarctic sea-ice were found by SSM/I (Willmes et al., 2009). AMSR-E/2 have more opportunities to identify these transitions due to the more appropriate local acquisition time. AMSR-E/2 36.5 GHz DAV in vertical polarization (DAV36), were used to detect the pan-Antarctic snowmelt and calculated as follows:

$$DAV36 = | Tb_{V36A} - Tb_{V36D}| \tag{2}$$

where Tb_{V36A} and Tb_{V36D} are the Tb_{V36} in ascending and descending passes respectively. Willmes et al. (2009) determined melt signals when the DAV37 of SSM/I exceeds 10 K. The threshold was validated against extensive field data on the Antarctic sea ice. We utilized the same threshold for melt detection based on AMSR-E/2 DAV36 considering the differences between AMSR-E 36 GHz Tb and SSM/I 37 GHz Tb are very small (Dai and Che, 2010). In the region south of 85° S where the surface snow is stable and never melts, the bias between the two measurements was only approximately 1 K during 2002-2003 (Supplement Fig. 1). Slight Tb offsets between different sensors should not affect the results when using temporal Tb variability in melt detection (Markus et al., 2009).

This method was also applied in the investigation of snow surface freeze/thaw cycles on the AIS. The verification of snowmelt is difficult, especially in the pan-Antarctic where meltwater refreezes quickly, and climatic data are sparse. However, surface snowmelt is determined by atmospheric conditions and agrees well with the Tair distribution pattern (Tedesco, 2007; Liang et al., 2013). In-situ Tair measurements at Zhongshan Station (69.37°S, 76.38°E) obtained from the Chinese National Arctic and Antarctic Data Center (www.chinare.org.cn) were used to evaluate the DAV36 algorithm (Fig. 21). The overall accuracy (p_0, the proportion of observed agreement) and Kappa coefficient $k = (p_0 – p_c)/(1- p_c)$ were used to measure the coincidence based on the confusion matrix, where p_c is the proportion in agreement due to chance (Cohen, 1960). Tb_{V36A} and Tb_{V36D} showed sharp increases at melt onset, while decreased below the winter mean in the late melt seasons with associated snow metamorphism. However, positive maximum Tair agreed well with melt signals (i.e., the presence of liquid water) determined by the DAV method, with an overall accuracy of 0.93 and a Kappa coefficient of 0.79.

When a snowpack on sea ice begins to melt, it appears as a blackbody at microwave wavelengths and the Tb increases sharply (Markus et al., 2009), while open water exhibits much lower Tb (Markus and Cavalieri, 1998). Therefore, Tb amplitudes may not be strong enough to be identified as melt signals for first-year sea ice with sufficient open water. To eliminate the effect of open water in melt detection, $DAV36_{ice}$ (i.e., DAV36 contributed by the ice-covered portion) was applied in the Antarctic sea ice snowmelt detection. Regardless of the atmospheric effects, the Tb of sea ice is comprised of the ice portion (Tb_{ice}) and open water portion (Tb_{ow}) (Markus and Cavalieri, 1998):

$$Tb= Tb_{ice}\ SIC+ Tb_{ow}\ (1-SIC) \tag{3}$$

therefore, $DAV36_{ice}$ can be calculated as follows:

$$DAV36_{ice} = \left| \frac{Tb_{V36A} - Tb_{ow}(1 - SIC_A)}{SIC_A} - \frac{Tb_{V36D} - Tb_{ow}(1 - SIC_D)}{SIC_D} \right| \tag{4}$$

where SIC_A and SIC_D represent the SIC for ascending and descending passes. If we assume that the SIC of the two passes remains unchanged (i.e., $SIC_A = SIC_D$), then we have:

$$DAV36_{ice} = \frac{\left| Tb_{V36A} - Tb_{V36D} \right|}{SIC} \tag{5}$$

5   Fig. 3 2 shows the comparison of meteorological observations of a sea ice buoy in the Weddell Sea and the corresponding AMSR2 measurements. Snow buoy observations (Fig. 3a2a), including snow depth and Tair, were obtained from the Alfred Wegener Institute (AWI, http://www.meereisportal.de/en/seaicemonitoring/buoy-mapsdata/). The inset map in Fig. 3b 2b illustrates the annual mean SIC and the route of the buoy from multi-year ice to first-year ice in the Weddell Sea. Tb_{V36A} and Tb_{V36D} showed great differences in the melt season. Sporadic melt events were detected before December 2014. Accompanied

10 by a slight decrease of snow depth, DAV36 exceeded 10 K and Tair went above the freezing point after mid-December. $DAV36_{ice}$ was nearly equal to DAV36 when SIC was above 90%, while it was much higher than the latter when the SIC dropped after February. DAV36 was below 10 K with Tair above the freezing point many times (see the black arrows), while these melt signals were successfully recognized by $DAV36_{ice}$ algorithm. The overall accuracy and Kappa coefficient between the positive maximum Tair and melt signals derived by satellites were 0.79 and 0.50+ based on the DAV36 algorithm, while

15 those were and 0.82 and 0.60 based on the $DAV36_{ice}$ algorithm, indicating a fair to good strength of agreement according to Fleiss et al. (2003). $DAV36_{ice}$ algorithm performs better than DAV36 algorithm in the marginal ice zone by reducing the effect of open water.

    Melt signals derived from the DAV method and the positive Tair from AWS were not always strictly connected (Figs. 1&2). The mismatches largely occur in the period with transient snowmelt when thaw/freeze status shifted quickly and in the

20 regions with plenty of open water (typical SIC < 90%). For the periods that were identified as thaw/freeze status for at least three days, satellite-derived melt signals showed close agreement (OA=0.87, Kappa=0.68) with that derived from Tair over the sea ice with SIC > 90%. The disagreements in the identification of transient melt events may result from inconsistent spatial and temporal resolutions. Validating the large-scale satellite-based estimation (25 km for AMSR-E/2) against station-based measurements is always challenging due to representativeness errors (Lyu et al., 2017). The daily maximum Tair was derived

25 from hourly Tair records, while only two daily satellite observations were used in the DAV method. In the marginal sea ice zone, ice disintegrates, brine and flooding effects may play an important role in seasonal and even diurnal sea ice Tb variations, further complicating the story (Smith, 1998; Willmes et al., 2009). In addition, snowmelt may occur when Tair is below the freezing point because of the penetration and absorption of solar radiation within the snowpack (Koh and Jordan, 1995). Markus et al. (2009) have determined the Arctic sea ice freeze/thaw states based on gridded Tair data set with a threshold of -

30 1°C. Melt timing derived from different approaches are supposed to show similar spatial distribution patterns. To evaluate the

7

performance of the DAV method on a larger scale, snowmelt over the pan-Antarctic was also determined by ERA-Interim reanalysis when the daily maximum Tair exceeded -1°C.

~~To capture complete melt seasons, a melting year begins on 1 July and ends on 30 June of the next year. The missing observations were filled based on time-line interpolation. Spurious Tb variations may occasionally be mistaken for melt signals, which can be caused by clouds, atmospheric water vapor, wind-induced surface roughening, and residual calibration errors. To mitigate their impacts on melt detection, a median filter with a 3×3 window was applied to the satellite observations. Further, melt detection was constrained to the days with compatible thermal regimes following Belchansky et al. (2004). The days with ERA-Interim Tair > -5°C were first determined, and the DAV36 algorithm was applied henceforth.~~

Considering the existence of both transient and persistent snowmelt in the pan-Antarctic, early melt onset (EMO, the first day when snowmelt is detected) and continuous melt onset (CMO, the first day when snowmelt lasts for at least three consecutive days) were investigated in this study. Melting days ~~was~~ were calculated by summing the number of days with snowmelt. Sufficient Antarctic sea ice melts quickly in austral summer and does not emerge again in the melting year. In such cases, the last day of snowmelt is always the day that ~~sea ice disappears~~SIC drops below 15%, rather than the day that freeze-up begins. Thus freeze-up and melt duration were not included in this study. Antarctic sea ice cover has exhibited considerable regional and annual variations (Hobbs et al., 2016). To be consistent, the melting days fraction (MDF) and melt extent fraction (MEF) were introduced to study the snowmelt variations:

$$MDF = \frac{\text{Melting days}}{\text{Ice cover days}}, \tag{6}$$

$$MEF = \frac{\text{Melt extent}}{\text{Ice cover extent}} \tag{7}$$

where ice cover was determined with SIC > 15% for sea ice, and the AIS is assumed to be ice-covered all the year.

~~Melt signals derived from the DAV method and the positive Tair from AWS were not always strictly connected (Figs. 3&4). Their differences may be attributed to inconsistent temporal resolutions because snowmelt and refreezing can occur at any time of the day. The daily maximum Tair was derived from hourly Tair records, while only two daily satellite observations were used in the DAV method. In addition, snowmelt may occur when Tair is below the freezing point because of the penetration and absorption of solar radiation within the snowpack (Koh and Jordan, 1995). Markus et al. (2009) have determined the Arctic sea ice freeze/thaw states based on gridded Tair data set with a threshold of -1°C. To evaluate the performance of the DAV method on a larger scale, snowmelt over the pan-Antarctic was also determined by ERA-interim reanalysis when the daily maximum Tair exceeded -1°C.~~

3.2. Data preprocessing and analysis

To capture complete melt seasons, a melting year begins on 1 July and ends on 30 June of the next year. The missing observations were filled based on time-line interpolation. Spurious Tb variations may occasionally be mistaken for melt signals, which can be caused by clouds, atmospheric water vapor, wind-induced surface roughening, and residual calibration errors.

5   To mitigate their impacts on melt detection, a median spatial filter with a 3×3 window was applied to the satellite observations. Further, melt detection was constrained to the days with compatible thermal regimes following Belchansky et al. (2004). The days with ERA-Interim Tair > -5°C were first determined, and the DAV36 algorithm was applied henceforth. Linear trends were calculated using a least-squares adjustment. The significance levels of the correlations and regressions were determined using the Student's t-tests.

10   To study the response of the pan-Antarctic surface snowmelt to circulation conditions, we explored the relationship between the melt indices and El Niño/Southern Oscillation (ENSO) and Southern Annular Mode (SAM). Nino3.4, the average sea surface temperature anomaly in the tropical (170°W–120°W, 5°S–5°N), is calculated from the Hadley Centre Sea Ice and Sea Surface Temperature dataset (Rayner et al., 2003). Southern Oscillation Index (SOI) is calculated using the pressure difference between Tahiti and Darwin (Ropelewski et al., 1987). Southern Annular Mode is calculated using the zonal pressure

15   difference between 40°S and 65°S (Marshall, 2003).

4 Results

4.1 Snowmelt distribution and trends

The study area was divided into six sub-areasparts to investigate regional discrepancies in surface snowmelt on sea ice and ice sheet according to Parkinson and Cavalieri (2012) (Fig. 43), namely, the Weddell Sea (WS, 60 °W to 20 °E), Indian Ocean

20   (IO, 20 °E to 90 °), Pacific Ocean (PO, 90 °E to 160 °E), Ross Sea (RS, 160 °E to 130 °W), Bellingshausen Amundsen Sea (BAS, 130 °W to 60 °W), and the AIS including all floating ice shelves.

Integrated pan-Antarctic annual melt indices were examined based on AMSR-E/2 (Fig. 54a-d). On average, pan-Antarctic EMO occurred on 24 September (DOY 86), CMO arrived 53 days later (16 November), and snowmelt lasted for 30 days during 2012-2017 (Table 1). In general, snowmelt shows significant latitudinal zonality. EMO and CMO occur later from the

25   marginal sea ice to the inland of the AIS, from low-latitudes to high-latitudes, while MDF increases in the opposite direction. In some parts of the marginal sea ice zone, EMO was later than that in higher altitudes. This is because sea ice did not occur in these regions until early September (Stammerjohn et al., 2008), while transient surface snowmelt can occur before that in August at lower latitudes (Supplement Fig. 2). However, the earliest CMO was still found in the marginal sea ice zone (Fig. 54b,d).

30   Annual mean EMO, CMO, melting days and MDF of the six sub-areasregions were also analyzed (Table 1). In terms of the satellite observations, the earliest EMO (15 August) and CMO (5 November) occurred in BAS where surface snow melted

for 37 days. As expected, snowmelt on the AIS began the latest with EMO occurring on 7 December and CMO occurring on 18 December. Sea ice surface snow in WS can melt for more than 100 days (Fig. ~~5c~~4c). MDF can reach 30% for the marginal sea ice in RS and WS (Fig. ~~5d~~4d). Snowmelt at high-latitudes was variable. For example, surface snowmelt on the Ross Ice Shelf extended to the inland area and even reached the Transantarctic Mountains in 2004-2005, but the Ross Ice Shelf was almost totally frozen during 2009-2011 (not shown).

Melting timing derived from AMSR-E/2 satellite observations and ERA-Interim reanalysis generally agreed well with each other in the AIS and IO, but showed some discrepancies in other regions (Table 1 and Fig. 4)~~The spatial distribution patterns of pan-Antarctic surface snowmelt derived from AMSR-E/2 and ERA generally agreed well with each other, especially for the AIS (Table 1 and Fig. 5)~~. On average, pan-Antarctic EMO and CMO derived by satellites were ~~12~~11 days and 27 days later than that detected by ERA-Interim. AMSR-E/2 detected later EMO on the near-shore sea ice, and later CMO in BAS and RS (Fig. ~~5~~4i,j). ERA-Interim recognized more melt events in WS (16 days), BAS (19 days), and RS (20 days), where intense surface snowmelt was found (Fig. ~~5~~4k). Satellite-based MDF for the marginal sea ice is lower than that derived by ERA-Interim (Fig. ~~5~~4l). With the exception of the Antarctic Peninsula where the melt season can last for more than three months, the AIS melt timings detected by the two methods were consistent with each other (Fig. ~~5~~4i-l).

The ~~S~~seasonal evolution of snowmelt in different regions was examined by the normalized histograms of annual mean EMO, CMO, melting days and MDF (Fig. ~~6~~5). Notable differences existed between the temporal distribution of sea ice and ice sheet melt patterns. Sea ice EMO concentrated in mid-July for BAS, and in early August for IO. By contrast, the frequency of AIS EMO did not reach the peak until early January. The occurrence of pan-Antarctic CMO peaked in December, varying from early December in BAS and WS to late December in the AIS. Melting days and MDF histograms indicate a large number of transient melt events, especially in the AIS. Approximately 16% of the AIS experienced snowmelt over 2002-2017; however, approximately 66% of these areas melted for no more than 5 days. In general, melting days seldom exceeded 45 d, with the exception of the BAS and WS where plenty of surface snow on sea ice can melt for more than two months. The annual mean MDF in the BAS was 17% (Table 1), while the MDF in most of the AIS was below 5% (Fig. ~~6~~5**)**.

The CMO histogram suggests that most of the pan-Antarctic continuous snowmelt began between October and January (Fig. ~~6~~5), corresponding to a sharp increase in MEF (Fig. ~~7~~6). In mid-January, most of the Antarctic sea ice experienced surface snowmelt, and the daily mean MEF can reach 80%. The AIS daily mean MEF was much lower and also reached a maximum (8%) in mid-January (Fig. ~~7~~6). MEF declined rapidly between late January and March. The Antarctic sea ice daily mean MEF declined to below 10% and the AIS became almost completely refrozen after April.

4.2 Trend analysis

Trends in surface melting conditions during 2002-2017 were analyzed. Linear trends ~~in the melt indices~~ for the pixels with continuous records were calculated based on the annual departures. EMO is not included in the trend analysis because of the chaotic spatial distribution of the early transient melt events. ~~As listed in Table 2, the pan-Antarctic snowmelt overall showed a significant trend (at the 90% confidence level) towards later EMO (0.68 days yr⁻¹), especially in the RS and BAS. Trends in~~

~~CMO, melting days and MDF were not statistically significant for the pan-Antarctic. EMO came significantly later (at the 99%~~
~~confidence level) in RS (1.72 days yr⁻¹). Melting days in RS was also significantly decreased (at the 90% confidence level).~~
~~The largest trend in EMO (2.13 days yr⁻¹) was observed in BAS. CMO occurred significantly earlier in WS and IO where MDF~~
~~also significantly increased. Melting days and MDF have both significantly increased (above the 95% confidence level) in PO.~~
5 ~~The AIS showed a negative trend in surface snowmelt with a later EMO and CMO, and slightly decreasing melting days and~~
~~MDF.~~

~~The inter-annual departures of melt indices for the pan-Antarctic, AIS and RS where the most significant change in~~
~~EMO was found are shown in Fig. 8. Melt indices showed considerable inter-annual variations. Pan-Antarctic EMO came~~
~~much later in recent years after reaching the earliest point in 2010-2011. RS and AIS presented negative trends in surface~~
10 ~~snowmelt, which were indicated by all the melt indices. The earliest EMO in RS was found in 2004-2005 when nearly the~~
~~entire Ross Ice Shelf experienced snowmelt. All the AIS snowmelt indices indicated the weakest melt season in 2014-2015.~~

~~The c~~Considerable decrease in surface snowmelt in the RS can ~~also~~ be clearly seen in Fig. ~~9~~7, which illustrates the
trends in melt indices during 2002-2017. No significant CMO trend was observed in most of the pan-Antarctic. ~~Most of the~~
~~pan-Antarctic showed a later EMO, especially in RS where melting days also~~ Melting days and MDF for the off-shore sea ice
15 in the RS presented remarkable negative trends. Surface snow on the East Antarctic sea ice, especially in PO, presented trends
towards increasing melting days and MDF ~~a later EMO. However, melting days and MDF in these regions have increased~~.
~~EMO and~~ CMO appeared earlier on the marginal sea ice in WS where melting days and MDF also significantly increased.
Many low-lying ice shelves in the AIS, such as the Larsen C Ice Shelf in the Antarctic Peninsula and the Abbot Ice Shelf in
Marie Byrd Land, presented trends towards decreasing melting days and MDF.

20 **4.2 Linkages between pan-Antarctic surface snowmelt and climate indices** ~~**5.3 Response of the pan-Antarctic surface**~~
~~**snowmelt to atmospheric indices**~~

Snowmelt in the pan-Antarctic was found to be strongly associated with ENSO and SAM~~the atmospheric component of the~~
~~El Niño Southern Oscillation (ENSO) and the Southern Annular Mode (SAM)~~ (Turner, 2004; Tedesco and Monaghan, 2009;
Oza et al., 2011; Meredith et al., 2017). In January 2016, the extensive surface snowmelt in West Antarctica was likely linked
25 with sustained and strong advection of warm marine air due to the concurrent strong El Nino event (Nicolas et al., 2017). The
weakly negative trend in surface temperature in Antarctica was consistent with the positive trends in SAM during summer and
autumn since the 1970s (Monaghan et al., 2008).

~~To study the response of the pan-Antarctic surface snowmelt to atmospheric conditions, we explored the relationship~~
~~between the melt indices and Nino3.4 (Rayner et al., 2003), Southern Oscillation Index (SOI) (Ropelewski et al., 1987) and~~
30 ~~SAM (Marshall, 2003)~~ The comparison between pan-Antarctic surface snowmelt and the climate indices are illustrated in
Table 2~~(Table 3)~~. The CMO of the pan-Antarctic was significantly correlated (at the 95% confidence level) with summer (DJF)
SAM. CMO and MDF were also well correlated with summer SAM in RS, BAS and AIS. The correlation coefficient between
EMO and SAM was the highest (0.77) in IO. CMO was significantly correlated with SOI and Nino3.4 in RS. Melting days

and MDF were also found to be strongly correlated with summer SOI or Nino3.4 in BAS where strong decreases in sea-ice concentration and duration were always linked with contemporary ENSO warm events (Kwok et al., 2002; Bromwich et al., 2004).

MDF was negatively related to summer SAM for off-shore sea ice in BAS and RS where MDF has significantly decreased (Fig. 8~~13~~). This relationship was especially significant in the AIS (R=-0.88, P<0.01). High anti-correlations were found between summer SAM and the annual mean MEF on the Antarctic sea ice and AIS (Fig. ~~13~~8b). The significantly decreased (at the 95% confidence level) annual mean melt extent on the AIS (-0.37×10^4 km^2 yr^{-1}) during 2002-2017 was strongly associated with increasing summer SAM (R=-0.82, P<0.01). This phenomenon is in line with the decreased surface snowmelt and the enhanced summer SAM in AIS since the 1970s (Marshall, 2003; Tedesco and Monaghan, 2009). The positive SAM results in anomalously strong westerlies over the Southern Ocean and hence the reduction in poleward heat transport, leading to the subsequent atmospheric cooling in the Antarctic regions (Thompson and Solomon, 2002). SAM is the principal driver of AIS near-surface temperature and snowmelt variability (Marshall, 2007; Tedesco and Monaghan, 2009). ~~, and it~~It is expected to have a continuous effect on the Antarctic climate in the next few decades considering the projected ozone recovery (Thompson et al., 2011).

5 Discussion

5.1 Comparisons

Tair above/below the freezing point does not always indicate a melting/frozen snowpack. EMO and CMO derived from ERA-Interim were earlier than that detected by AMSR-E/2 data (Fig. ~~5~~ 4 and Table 1). This is because it takes time to produce liquid water when snow temperature approaches the melting point ~~(Markus et al., 2009)~~. Daily Tb variation is limited when liquid water does not refreeze or snowpack is still melting in the warm nights during heavy melt seasons (Willmes et al., 2009; Semmens and Ramage, 2014). As a result, ERA-Interim recognized more melt events for the regions where heavy snowmelt was found and the DAV method fails to work, such as the WS, BAS, RS and the Larsen C ice shelf. Th~~is~~e might also be the reason that the melt onset was very early in RS while few melt events were detected by AMSR-E/2.

Willmes et al. (2009) established the SSM/I DAV method to study the Antarctic sea ice CMO (hereafter W09). Antarctic sea ice CMO mapped by AMSR-E shows a higher spatial continuity than that in W09. CMO derived from the two satellites agreed well with each other at high latitudes during 2002-2008. However, W09 found a remarkably later CMO on the marginal sea ice compared with results from AMSR-E (Fig. ~~10~~9). There are several reasons for the significant difference in marginal sea ice CMO detected by AMSR-E and SSM/I data. First, W09 only studied surface snowmelt on sea ice after 1 October, while the melt season begins on 1 July in this study. Second, the DAV36$_{ice}$ algorithm can amplify snowmelt signals by reducing the effect of open water, so that more melt events can be recognized (Fig. ~~3~~2). Third, compared with SSM/I, AMSR-E operated in a stable orbit and observed the pan-Antarctic with more appropriate local acquisition time, and hence had more opportunities to identify melt events (Supplement Fig. 2).

Considering that snowmelt can be biased by various SMMR and SSM/I acquisition times, Picard and Fily (2006) retrieved the AIS surface snowmelt based on corrected 18-19 GHz Tb time series (hereafter PF06). The AIS daily melt extent derived by AMSR-E/2 and ERA-Interim were consistent with each other with R^2=0.92. The PF06 daily melt extent also presented a high correlation with results from AMSR-E/2 (R^2=0.77). However, the melt extent derived by PF06 was significantly smaller

5   than that mapped by AMSR-E/2 (Fig. ~~11~~10a). AMSR-E/2 and ERA-Interim daily mean melt extent were more than twice the melt extent mapped by PF06 from December to February (Fig. ~~11~~10b). In a recent study, PF06 melt extent was also found to be much smaller compared with that derived from scatterometers (Zheng et al., 2020). PF06 determined snowmelt when the SSM/I 19 GHz Tb exceeds the winter mean plus 2.5 times the standard deviation of the winter Tb. During the melt seasons, Tb may decrease due to the strong volume scattering resulting from the increase of snow grain size and the formation of icy

10   layers ~~snow metamorphism~~ (Ramage and Isacks, 2002; Markus et al., 2009). Summer Tb can even be much lower than the winter observations (Zheng et al., 2018). Therefore, PF06 may underestimate surface snowmelt when snow metamorphism occurs in melt season. The DAV method is unaffected by snow metamorphism but may fail to work when liquid water does not refreeze or snowpack is still melting in warm nights (Willmes et al., 2009). Fortunately, the Antarctic surface snowmelt is always short-lived and can refreeze quasi-instantaneously (Zheng et al., 2018; van den Broeke et al., 2010a). ~~PF06 determined~~

15   ~~snowmelt when the SSM/I 19 GHz Tb exceeds the winter mean plus 2.5 times the standard deviation of the winter Tb; therefore, it may underestimate surface snowmelt. Moreover, as explained in Section 3.1 and as shown in Fig. 1, Tb decreases during the energy dampening phase. Single-channel methods such as PF06 may miss the melt signals during a heavy melt season, while the DAV method is unaffected by snow metamorphism and can detect snowmelt even during the energy dampening phase.~~

5.2 Uncertainties

20   There are several uncertainties in the pan-Antarctic snowmelt derived from AMSR-E/2 data. First, the ~~DAV method may fail to work when liquid water does not refreeze or snowpack is still melting in warm nights (Willmes et al., 2009). The~~ regions with snowmelt that became more prevalent would presumably show a decrease in melting days based on the DAV method when snowmelt even occurs in the night. ~~Fortunately, unlike the Arctic, surface snowmelt on the Antarctic sea ice is always patchy and relatively short-lived (Drinkwater and Liu, 2000).~~ Second, although the DAV method used in this study performs

25   well when compared with meteorological observations, the optimal threshold may differ temporally and regionally with varying snow properties. ~~In addition, ice disintegrates, brine and flooding effects may play an important role in seasonal and even diurnal sea-ice Tb variations, further complicating the story (Smith, 1998; Willmes et al., 2009).~~ Arndt et al. (2016) utilized individual local thresholds with a median value of 6 K to detect snowmelt based on SSM/I DAV and recognized an earlier melt onset than W09. Melt indices derived from the DAV method showed considerable variations when applying

30   different thresholds (from 6 to 14 K in Fig. ~~11~~12). Varying the threshold applied to AMSR-E/2 DAV by ±4 K results in -17 days to 14 days departure for the annual mean EMO, and -9 days to 12 days departure for annual mean melting days.

It should be noted that the presence of snow liquid water detected by AMSR-E/2 does not necessarily mean that the snowpack is melting because it takes time for meltwater to refreeze. In addition, after refreezing of surface snow, subsurface

liquid water can still be detected by radiometer due to the penetrating capacity of microwaves (Ashcraft and Long, 2006). The DAV36$_{ice}$ algorithm for sea ice snowmelt detection assumes that the SIC of the two passes remains unchanged, which may not be true and lead to misidentifications of melt signals due to quick sea ice drift and disintegration. The algorithm can be further improved if the twice-daily SIC product is available in the future. Though AMSR-E/2 observed the pan-Antarctic at the appropriate time for snowmelt detection, they may underestimate snowmelt because snowmelt can occur at any time and refreezing can be quasi-instantaneous. Other sources of the microwave remote sensing data set, such as scatterometer and synthetic aperture radar, are expected to enrich daily observations in future works. Snowmelt derived by satellites can serve as input and output validations for climate models.

5.3 Response of the pan-Antarctic surface snowmelt to atmospheric indices

Snowmelt in the pan-Antarctic was found to be strongly associated with the atmospheric component of the El-Niño Southern Oscillation (ENSO) and the Southern Annular Mode (SAM) (Turner, 2004; Tedesco and Monaghan, 2009; Oza et al., 2011; Meredith et al., 2017). In January 2016, the extensive surface snowmelt in West Antarctica was likely linked with sustained and strong advection of warm marine air due to the concurrent strong El Nino event (Nicolas et al., 2017). The weakly negative trend in surface temperature in Antarctica was consistent with the positive trends in SAM during summer and autumn since the 1970s (Monaghan et al., 2008).

To study the response of the pan-Antarctic surface snowmelt to atmospheric conditions, we explored the relationship between the melt indices and Nino3.4 (Rayner et al., 2003), Southern Oscillation Index (SOI) (Ropelewski et al., 1987) and SAM (Marshall, 2003) (Table 3). The CMO of the pan-Antarctic was significantly correlated (at the 95% confidence level) with summer (DJF) SAM. CMO and MDF were also well correlated with summer SAM in RS, BAS and AIS. The correlation coefficient between EMO and SAM was the highest (0.77) in IO. CMO was significantly correlated with SOI and Nino3.4 in RS. Melting days and MDF were also found to be strongly correlated with summer SOI or Nino3.4 in BAS where strong decreases in sea-ice concentration and duration were always linked with contemporary ENSO warm events (Kwok et al., 2002; Bromwich et al., 2004).

MDF was negatively related to summer SAM for off-shore sea ice in BAS and RS where MDF has significantly decreased (Fig. 13). This relationship was especially significant in the AIS (R=-0.88, P<0.01). High anti-correlations were found between summer SAM and the annual mean MEF on the Antarctic sea ice and AIS (Fig. 13b). The significantly decreased (at the 95% confidence level) annual mean melt extent on the AIS (-0.37×10⁴ km² yr⁻¹) during 2002-2017 was strongly associated with increasing summer SAM (R=-0.82, P<0.01). This phenomenon is in line with the decreased surface snowmelt and the enhanced summer SAM in AIS since the 1970s (Marshall, 2003; Tedesco and Monaghan, 2009). The positive SAM results in anomalously strong westerlies over the Southern Ocean and hence the reduction in poleward heat transport, leading to the subsequent atmospheric cooling in the Antarctic regions (Thompson and Solomon, 2002). SAM is the principal driver of AIS near-surface temperature and snowmelt variability (Marshall, 2007; Tedesco and Monaghan, 2009), and it is expected to have

14

6 Conclusions

5 In this study, we investigated the pan-Antarctic surface melting conditions during 2012-2017 by using daily AMSR-E/2 observations~~Tb variations~~. Compared with SSM/I, the more stable orbit and more appropriate local acquisition time of AMSR-E/2 enable us to take full advantage of the brightness temperature variations~~DAV method~~ to investigate surface melt events. The performance of this method was improved in the marginal sea ice zone by excluding the effect of open water. Although ~~the DAV~~ this method may fail to recognize melt events when meltwater does not refreeze or snowpack melts in the warm nights, snowmelt detected by AMSR-E/2 agreed well with the in-situ positive Tair observations, and was more extensive than

10 that detected by SSM/I.

Pan-Antarctic snowmelt showed significant latitudinal zonality. On average, early snowmelt begins in late September, while continuous snowmelt begins in mid-November. Sea ice in ~~WS~~ the Weddell Sea can melt for more than 100 days. Snowmelt on the Antarctic sea ice and ~~AIS~~ Antarctic Ice Sheet exhibited great differences in temporal distribution patterns. ~~The pan-Antarctic showed a significant trend (at the 90% confidence level) towards later EMO (0.68 days yr⁻¹).~~ Negative

15 trends in snowmelt were found in ~~RS~~ the Ross Sea and ~~AIS~~Antarctic Ice Sheet. ~~CMO~~ Continuous melt onset in the pan-Antarctic was well correlated with summer Southern Annular Mode~~SAM~~. The decreasing surface snowmelt in the Antarctic Ice Sheet~~AIS~~ was very likely linked with the positive summer Southern Annular Mode~~SAM trend~~ during 2002-2017.

~~Though AMSR-E/2 observed the pan-Antarctic at the appropriate time for snowmelt detection, they may underestimate snowmelt because snowmelt can occur at any time and refreezing can be quasi-instantaneous. Other sources of the microwave~~

20 ~~remote sensing data set, such as scatterometer and synthetic aperture radar, are expected to enrich daily observations in future works. Snowmelt derived by satellites can serve as input and output validations for climate models.~~

References

Abdalati, W. and Steffen, K.: Passive microwave-derived snow melt regions on the Greenland Ice Sheet, Geophys. Res. Lett., 22(7), 787–790, doi:10.1029/95GL00433, 1995.

Ackley, S. F., Lewis, M. J., Fritsen, C. H. and Xie, H.: Internal melting in Antarctic sea ice: Development of "gap layers,"
10   Geophys. Res. Lett., 35, L11503, doi:10.1029/2008GL033644, 2008.

Arndt, S., Willmes, S., Dierking, W. and Nicolaus, M.: Timing and regional patterns of snowmelt on Antarctic sea ice from passive microwave satellite observations, J. Geophys. Res. Ocean., 121(8), 5916–5930, doi:10.1002/2015JC011504, 2016.

Ashcraft, I. S. and Long, D. G.: Comparison of methods for melt detection over Greenland using active and passive microwave measurements, Int. J. Remote Sens., 27(12), 2469–2488, doi:10.1080/01431160500534465, 2006.

15   Belchansky, G. I., Douglas, D. C. and Platonov, N. G.: Duration of the Arctic sea ice melt season: Regional and interannual variability, 1979-2001, J. Clim., 17(1), 67–80, doi:10.1175/1520-0442(2004)017<0067:DOTASI>2.0.CO;2, 2004.

Bell, R. E., Banwell, A. F., Trusel, L. D. and Kingslake, J.: Antarctic surface hydrology and impacts on ice-sheet mass balance, Nat. Clim. Chang., 8(12), 1044–1052, doi:10.1038/s41558-018-0326-3, 2018.

Bliss, A., Miller, J. and Meier, W.: Comparison of Passive Microwave-Derived Early Melt Onset Records on Arctic Sea Ice,
20   Remote Sens., 9(3), 199, doi:10.3390/rs9030199, 2017.

Brandt, R. E., Warren, S. G., Worby, A. P. and Grenfell, T. C.: Surface albedo of the Antarctic sea ice zone, J. Clim., 18(17), 3606–3622, doi:10.1175/JCLI3489.1, 2005.

Bromwich, D. H., Monaghan, A. J. and Guo, Z.: Modeling the ENSO modulation of Antarctic climate in the late 1990s with the Polar MM5, J. Clim., 17(1), 109–132, doi:10.1175/1520-0442(2004)017<0109:MTEMOA>2.0.CO;2, 2004.

25   Brucker, L., Picard, G. and Fily, M.: Snow grain-size profiles deduced from microwave snow emissivities in Antarctica, J. Glaciol., 56(197), 514–526, doi:10.3189/002214310792447806, 2010.

Cohen, J.: A Coefficient of Agreement for Nominal Scales, Educ. Psychol. Meas., 20(1), 37–46, doi:10.1177/001316446002000104, 1960.

Comiso, J.: Bootstrap Sea Ice Concentrations from Nimbus-7 SMMR and DMSP SSM/I-SSMIS, Version 3. NASA National
30   Snow and Ice Data Center Distributed Active Archive Center, NSIDC, doi:10.5067/7Q8HCCWS4I0R, 2017.

Comiso, J. C. and Nishio, F.: Trends in the sea ice cover using enhanced and compatible AMSR-E, SSM/I, and SMMR data, J. Geophys. Res., 113, C02S07, doi:10.1029/2007JC004257, 2008.

Dai, L. and Che, T.: Cross-platform calibration of SMMR, SSM/I and AMSR-E passive microwave brightness temperature, Sixth Int. Symp. Digit. Earth Data Process. Appl., 7841, 784103, doi:10.1117/12.873150, 2010.

Dee, D. P., Uppala, S. M., Simmons, A. J., Berrisford, P., Poli, P., Kobayashi, S., Andrae, U., Balmaseda, M. A., Balsamo, G., Bauer, P., Bechtold, P., Beljaars, A. C. M., van de Berg, L., Bidlot, J., Bormann, N., Delsol, C., Dragani, R., Fuentes, M., Geer, A. J., Haimberger, L., Healy, S. B., Hersbach, H., Hólm, E. V., Isaksen, L., Kållberg, P., Köhler, M., Matricardi, M., McNally, A. P., Monge-Sanz, B. M., Morcrette, J.-J., Park, B.-K., Peubey, C., de Rosnay, P., Tavolato, C., Thépaut, J.-N. and Vitart, F.: The ERA-Interim reanalysis: configuration and performance of the data assimilation system, Q. J. R. Meteorol. Soc., 137(656), 553–597, doi:10.1002/qj.828, 2011.

Drinkwater, M. R. and Liu, X.: Seasonal to interannual variability in Antarctic sea-ice surface melt, IEEE Trans. Geosci. Remote Sens., 38(4), 1827–1842, doi:10.1109/36.851767, 2000.

Hall, D. K., Nghiem, S. V., Schaaf, C. B., DiGirolamo, N. E. and Neumann, G.: Evaluation of surface and near-surface melt characteristics on the Greenland ice sheet using MODIS and QuikSCAT data, J. Geophys. Res. Earth Surf., 114, F04006, doi:10.1029/2009JF001287, 2009.

Hobbs, W. R., Massom, R., Stammerjohn, S., Reid, P., Williams, G. and Meier, W.: A review of recent changes in Southern Ocean sea ice, their drivers and forcings, Glob. Planet. Change, 143, 228–250, doi:10.1016/J.GLOPLACHA.2016.06.008, 2016.

Intergovernmental Panel on Climate Change (IPCC): Climate change 2013: the physical science basis. Fifth assessment report of the intergovernmental panel on climate change, 2014.

Joshi, M., Merry, C. J., Jezek, K. C. and Bolzan, J. F.: An edge detection technique to estimate melt duration, season and melt extent on the Greenland Ice Sheet using Passive Microwave Data, Geophys. Res. Lett., 28(18), 3497–3500, doi:10.1029/2000gl012503, 2001.

Kang, D. H., Barros, A. P. and Dery, S. J.: Evaluating Passive Microwave Radiometry for the Dynamical Transition From Dry to Wet Snowpacks, IEEE Trans. Geosci. Remote Sens., 52(1), 3–15, 2014.

Knowles, M., Armstrong, R. and Brodzik, M. J.: AMSR-E/Aqua Daily EASE-Grid Brightness Temperatures, Version 1. Boulder, Colorado USA. NASA National Snow and Ice Data Center Distributed Active Archive Center, NSIDC, doi:https://doi.org/10.5067/RRR4WWORG070, 2006.

Koh, G. and Jordan, R.: Sub-surface melting in a seasonal snow cover, J. Glaciol., 41(139), 474–482, doi:10.3189/S002214300003481X, 1995.

Kwok, R., Comiso, J. C., Kwok, R. and Comiso, J. C.: Southern Ocean Climate and Sea Ice Anomalies Associated with the Southern Oscillation, J. Clim., 15(5), 487–501, doi:10.1175/1520-0442(2002)015<0487:SOCASI>2.0.CO;2, 2002.

Liang, L., Guo, H., Li, X. and Cheng, X.: Automated ice-sheet snowmelt detection using microwave radiometer measurements, Polar Res., 32(1), 1–13, doi:10.3402/polar.v32i0.19746, 2013.

Liu, H., Wang, L. and Jezek, K. C.: Wavelet-transform based edge detection approach to derivation of snowmelt onset, end and duration from satellite passive microwave measurements, Int. J. Remote Sens., 26(21), 4639–4660,

doi:10.1080/01431160500213342, 2005.

Lyu, H., Mccoll, K. A., Li, X., Derksen, C., Berg, A., Black, T. A., Euskirchen, E., Loranty, M., Pulliainen, J., Rautiainen, K., Rowlandson, T., Roy, A., Royer, A., Langlois, A., Stephens, J., Lu, H. and Entekhabi, D.: Validation of the SMAP freeze/thaw product using categorical triple collocation, Remote Sens. Environ., 205, 329–337, doi:10.1016/j.rse.2017.12.007, 2017.

Markus, T. and Cavalieri, D. J.: Snow Depth Distribution Over Sea Ice in the Southern Ocean from Satellite Passive Microwave Data, in Antarctic Sea Ice: Physical Processes, Interactions and Variability, vol. 74, pp. 19–39., 1998.

Markus, T., Stroeve, J. C. and Miller, J.: Recent changes in Arctic sea ice melt onset, freezeup, and melt season length, J. Geophys. Res. Ocean., 114, C12024, doi:10.1029/2009JC005436, 2009.

Marshall, G. J.: Trends in the Southern Annular Mode from observations and reanalyses, J. Clim., 16(24), 4134–4143, doi:10.1175/1520-0442(2003)016<4134:TITSAM>2.0.CO;2, 2003.

Marshall, G. J.: Half-century seasonal relationships between the Southern Annular Mode and Antarctic temperatures, Int. J. Climatol., 27(3), 373–383, doi:10.1002/joc.1407, 2007.

Matear, R. J., O'Kane, T. J., Risbey, J. S. and Chamberlain, M.: Sources of heterogeneous variability and trends in Antarctic sea-ice, Nat. Commun., 6, 8656, doi:10.1038/ncomms9656, 2015.

Meier, W. N. and Stroeve, J.: Comparison of sea-ice extent and ice-edge location estimates from passive microwave and enhanced-resolution scatterometer data, Ann. Glaciol., 48, 65–70, doi:10.3189/172756408784700743, 2008.

Meredith, M. P., Stammerjohn, S. E., Venables, H. J., Ducklow, H. W., Martinson, D. G., Iannuzzi, R. A., Leng, M. J., van Wessem, J. M., Reijmer, C. H. and Barrand, N. E.: Changing distributions of sea ice melt and meteoric water west of the Antarctic Peninsula, Deep Sea Res. Part 2. Top. Stud. Oceanogr., 139, 40–57, doi:10.1016/j.dsr2.2016.04.019, 2017.

Monaghan, A. J., Bromwich, D. H., Chapman, W. and Comiso, J. C.: Recent variability and trends of Antarctic near-surface temperature, J. Geophys. Res. Atmos., 113, D04105, doi:10.1029/2007JD009094, 2008.

Mote, T. L. and Anderson, M. R.: Variations in snowpack melt on the Greenland ice sheet based on passive-microwave measurements, J. Glaciol., 41(137), 51–60, 1995.

Nicolas, J. P., Vogelmann, A. M., Scott, R. C., Wilson, A. B., Cadeddu, M. P., Bromwich, D. H., Verlinde, J., Lubin, D., Russell, L. M., Jenkinson, C., Powers, H. H., Ryczek, M., Stone, G. and Wille, J. D.: January 2016 extensive summer melt in West Antarctica favoured by strong El Niño, Nat. Commun., 8, 15799, doi:10.1038/ncomms15799, 2017.

Oza, S. R., Singh, R. K. K., Vyas, N. K. and Sarkar, A.: Study of inter-annual variations in surface melting over Amery Ice Shelf, East Antarctica, using space-borne scatterometer data, J. Earth Syst. Sci., 120(2), 329–336, 2011.

Parkinson, C. L. and Cavalieri, D. J.: Antarctic sea ice variability and trends, 1979–2010, Cryosph., 6, 871–880, doi:10.5194/tc-6-871-2012, 2012.

Picard, G. and Fily, M.: Surface melting observations in Antarctica by microwave radiometers: Correcting 26-year time series from changes in acquisition hours, Remote Sens. Environ., 104(3), 325–336, 2006.

Picard, G., Fily, M. and Gallee, H.: Surface melting derived from microwave radiometers: A climatic indicator in Antarctica,

Ann. Glaciol., 46, 29–34, doi:10.3189/172756407782871684, 2007.

Powell, D. C., Markus, T., Cavalieri, D. J. and Gasiewski, A. J.: Microwave Signatures of Snow on Sea Ice: Modeling, IEEE Trans. Geosci. Remote Sens., 44(11), 3091–3102, 2006.

Ramage, J. M. and Isacks, B. L.: Determination of melt-onset and refreeze timing on southeast Alaskan icefields using SSM/I diurnal amplitude variations, Ann. Glaciol., 34, 391–398, doi:10.3189/172756402781817761, 2002.

Ramage, J. M. and Isacks, B. L.: Interannual variations of snowmelt and refreeze timing on southeast-Alaskan icefields, U.S.A., J. Glaciol., 49(164), 102–116, doi:10.3189/172756503781830908, 2003.

Rayner, N. A., Parker, D. E., Horton, E. B., Folland, C. K., Alexander, L. V., Rowell, D. P., Kent, E. C. and Kaplan, A.: Global analyses of sea surface temperature, sea ice, and night marine air temperature since the late nineteenth century, J. Geophys. Res., 108(D14), 4407, doi:10.1029/2002JD002670, 2003.

Ridley, J.: Surface melting on Antarctic Peninsula ice shelves detected by passive microwave sensors, Geophys. Res. Lett., 20(23), 2639–2642, doi:10.1029/93GL02611, 1993.

Ropelewski, C. F., Jones, P. D., Ropelewski, C. F. and Jones, P. D.: An Extension of the Tahiti–Darwin Southern Oscillation Index, Mon. Weather Rev., 115(9), 2161–2165, doi:10.1175/1520-0493(1987)115<2161:AEOTTS>2.0.CO;2, 1987.

Scambos, T., Hulbe, C., Fahnestock, M. and Bohlander, J.: The link between climate warning and break-up of ice shelves in the Antarctic Peninsula, J. Glaciol., 46(154), 516–530, doi:10.3189/172756500781833043, 2000.

Scott, R. C., Nicolas, J. P., Bromwich, D. H., Norris, J. R. and Lubin, D.: Meteorological Drivers and Large-Scale Climate Forcing of West Antarctic Surface Melt, J. Clim., 32(3), 665–684, doi:10.1175/JCLI-D-18-0233.1, 2018.

Semmens, K. and Ramage, J.: Melt patterns and dynamics in Alaska and Patagonia derived from passive microwave brightness temperatures., Remote Sens., 6(1), 603–620, doi:10.3390/rs6010603, 2014.

Serreze, M. G., Maslanik, J. A., Scharfen, G. R., Barry, R. G. and Robinson, D. A.: Interannual variations in snow melt over Arctic sea ice and relationships to atmospheric forcings, Ann. Glaciol., 17, 327–331, doi:10.3189/S0260305500013057, 1993.

Smith, D. M.: Observation of perennial Arctic sea ice melt and freeze-up using passive microwave data, J. Geophys. Res. Ocean., 103(C12), 27753–27769, doi:10.1029/98JC02416, 1998.

Stammerjohn, S. E., Martinson, D. G., Smith, R. C., Yuan, X. and Rind, D.: Trends in Antarctic annual sea ice retreat and advance and their relation to El Niño–Southern Oscillation and Southern Annular Mode variability, J. Geophys. Res., 113, C03S90, doi:10.1029/2007JC004269, 2008.

Steffen, K.: Surface energy exchange at the equilibrium line on the Greenland ice sheet during onset of melt, Ann. Glaciol., 21, 13–18, 1995.

Stroeve, J. C., Markus, T., Boisvert, L., Miller, J. and Barrett, A.: Changes in Arctic melt season and implifications for sea ice loss, Geophys. Res. Lett., 41, 1216–1225, doi:10.1002/2013GL058951.Received, 2014.

Stroeve, J. C., Mioduszewski, J. R., Rennermalm, A., Boisvert, L. N., Tedesco, M. and Robinson, D.: Investigating the Local Scale Influence of Sea Ice on Greenland Surface Melt, Cryosph., 11, 2363–2381, doi:10.5194/tc-2017-65, 2017.

Sundal, A. V., Shepherd, A., Nienow, P., Hanna, E., Palmer, S. and Huybrechts, P.: Melt-induced speed-up of Greenland ice sheet offset by efficient subglacial drainage, Nature, 469(7331), 521–524, doi:10.1038/nature09740, 2011.

Tanaka, Y., Tateyama, K., Kameda, T. and Hutchings, J. K.: Estimation of melt pond fraction over high-concentration Arctic sea ice using AMSR-E passive microwave data, J. Geophys. Res. Ocean., 121(9), 7056–7072, doi:10.1002/2016JC011876, 2016.

Tedesco, M.: Snowmelt detection over the Greenland ice sheet from SSM/I brightness temperature daily variations, Geophys. Res. Lett., 34, L02504, doi:10.1029/2006GL028466, 2007.

Tedesco, M.: Assessment and development of snowmelt retrieval algorithms over Antarctica from K-band spaceborne brightness temperature (1979-2008), Remote Sens. Environ., 113(5), 979–997, doi:10.1016/j.rse.2009.01.009, 2009.

Tedesco, M. and Monaghan, A. J.: An updated Antarctic melt record through 2009 and its linkages to high-latitude and tropical climate variability, Geophys. Res. Lett., 36, L18502, doi:10.1029/2009GL039186, 2009.

Tedesco, M., Abdalati, W. and Zwally, H. J.: Persistent surface snowmelt over Antarctica (1987–2006) from 19.35 GHz brightness temperatures, Geophys. Res. Lett., 34, L18504, doi:10.1029/2007gl031199, 2007.

The IMBIE team: Mass balance of the Antarctic Ice Sheet from 1992 to 2017, Nature, 558(7709), 219–222, doi:10.1038/s41586-018-0179-y, 2018.

Thompson, D. W. J. and Solomon, S.: Interpretation of recent Southern Hemisphere climate change, Science, 296(5569), 895–899, doi:10.1126/science.1069270, 2002.

Thompson, D. W. J., Solomon, S., Kushner, P. J., England, M. H., Grise, K. M. and Karoly, D. J.: Signatures of the Antarctic ozone hole in Southern Hemisphere surface climate change, Nat. Geosci., 4(11), 741–749, doi:10.1038/ngeo1296, 2011.

Turner, J.: The El Niño-Southern Oscillation and Antarctica, Int. J. Climatol., 24(1), 1–31, doi:10.1002/joc.965, 2004.

van den Broeke, M.: Strong surface melting preceded collapse of Antarctic Peninsula ice shelf, Geophys. Res. Lett., 32, L12815, doi:10.1029/2005GL023247, 2005.

van den Broeke, M., Bamber, J., Ettema, J., Rignot, E., Schrama, E., van de Berg, W., van Meijgaard, E., Velicogna, I. and Bert, W.: Partitioning recent Greenland mass loss, Science, 326(5955), 984–986, doi:10.1126/science.1178176, 2009.

van den Broeke, M., König-Langlo, G., Picard, G., Kuipers Munneke, P. and Lenaerts, J.: Surface energy balance, melt and sublimation at Neumayer Station, East Antarctica, Antarct. Sci., 22(1), 87–96, doi:10.1017/S0954102009990538, 2010a.

van den Broeke, M., Bus, C., Ettema, J. and Smeets, P.: Temperature thresholds for degree-day modelling of Greenland ice sheet melt rates, Geophys. Res. Lett., 37, L18501, doi:10.1029/2010GL044123, 2010b.

Wang, L., Toose, P., Brown, R. and Derksen, C.: Frequency and distribution of winter melt events from passive microwave satellite data in the pan-Arctic, Cryosph., 10, 2589–2602, doi:10.5194/tc-10-2589-2016, 2016.

Wiesmann, A. and Mätzler, C.: Microwave emission model of layered snowpacks, Remote Sens. Environ., 70(3), 307–316, doi:10.1016/S0034-4257(99)00046-2, 1999.

Willmes, S., Bareiss, J., Haas, C. and Nicolaus, M.: The importance of diurnal processes for the Seasonal cycle of Sea-ice microwave brightness temperatures during early Summer in the Weddell Sea, Antarctica, Ann. Glaciol., 44, 297–302,

doi:10.3189/172756406781811817, 2006.

Willmes, S., Haas, C., Nicolaus, M. and Bareiss, J.: Satellite microwave observations of the interannual variability of snowmelt on sea ice in the Southern Ocean, J. Geophys. Res., 114, C03006, doi:10.1029/2008JC004919, 2009.

Winebrenner, D. P., Nelson, E. D., Colony, R. and West, R. D.: Observation of melt onset on multiyear Arctic sea ice using the ERS 1 synthetic aperture radar, J. Geophys. Res., 99(C11), 22425–22441, doi:10.1029/94JC01268, 1994.

Zheng, L., Zhou, C., Liu, R. and Sun, Q.: Antarctic Snowmelt Detected by Diurnal Variations of AMSR-E Brightness Temperature, Remote Sens., 10(9), 1391, doi:10.3390/rs10091391, 2018.

Zheng, L., Zhou, C. and Liang, Q.: Variations in Antarctic Peninsula snow liquid water during 1999–2017 revealed by merging radiometer, scatterometer and model estimations, Remote Sens. Environ., 232, 111219, doi:10.1016/j.rse.2019.111219, 2019.

Zheng, L., Zhou, C. and Wang, K.: Enhanced winter snowmelt in the Antarctic Peninsula: Automatic snowmelt identification from radar scatterometer, Remote Sens. Environ., 246, 111835, doi:10.1016/j.rse.2020.111835, 2020.

Zwally, H. J.: Microwave Emissivity and Accumulation Rate of Polar Firn, J. Glaciol., 18(79), 195–215, doi:10.3189/S0022143000021304, 1977.

Zwally, H. J. and Fiegles, S.: Extent and duration of Antarctic surface melting, J. Glaciol., 40(136), 463–475, doi:10.1017/S0022143000012338, 1994.

Zwally, H. J., Abdalati, W., Herring, T., Larson, K., Saba, J. and Steffen, K.: Surface Melt-Induced Acceleration of Greenland Ice-Sheet Flow, Science, 297(5579), 218–222, doi:10.1126/science.1072708, 2002.

Table 1. Annual mean and standard deviation of pan-Antarctic EMO, CMO, melting days and MDF derived by AMSR-E/2 and ERA-Interim.

Observation	Melt index	WS	IO	PO	RS	BAS	AIS	All
AMSR-E/2	EMO (DOY)	24 Sep (86)±8	22 Sep (84)±6	4 Sep (66)±10	11 Sep (73)±8	15 Aug (46)±15	7 Dec (160)±6	24 Sep (86)±5
	CMO (DOY)	12 Nov (135)±7	19 Nov (142)±5	15 Nov (138)±6	14 Nov (137)±10	5 Nov (128)±12	18 Dec (171)±3	16 Nov (139)±4
	Melting days (days)	34±3	21±4	34±4	30±4	37±4	25±3	30±2
	MDF (%)	15±1	11±1	14±1	13±1	17±1	7±1	13±1
ERA-Interim	EMO (DOY)	9 Sep (71)±11	16 Sep (78)±16	25 Aug (56)±14	23 Aug (54)±9	28 Jul (28)±10	3 Dec (156)±5	12 Sep (74)±6
	CMO (DOY)	22 Oct (114)±11	9 Nov (132)±10	22 Oct (114)±12	29 Sep (91)±10	7 Sep (69)±16	10 Dec (163)±6	20 Oct (112)±7
	Melting days (days)	49±3	26±4	41±5	50±3	56±6	26±2	42±2
	MDF (%)	21±1	13±2	16±2	22±2	26±2	7±1	18±1

Melt index	WS	IO	PO	RS	BAS	AIS	All
EMO (days yr^{-1})	-0.35±1.10	0.09±0.82	1.37±1.40	1.72±0.71***	2.13±1.88*	0.71±0.76	0.68±0.59*
CMO (days yr^{-1})	-0.82±0.72*	-0.84±0.51**	-0.16±0.71	0.52±1.23	0.59±1.74	0.22±0.51	-0.22±0.43
Melting days (days yr^{-1})	0.34±0.33*	0.37±0.42	0.80±0.46***	-0.52±0.43*	-0.05±0.57	-0.33±0.41	0.11±0.20
MDF (% yr^{-1})	0.20±0.14**	0.15±0.14*	0.19±0.12**	-0.14±0.14	0.02±0.19	-0.09±0.11	0.07±0.08

5

10   **Table 23. Correlation between snowmelt index and ~~atmospheric~~ climate index for the Period 2002–2017. Correlation coefficients with *, ** and *** indicate statistical significance at 90%, 95%, and 99% confidence levels, respectively.**

~~Atmospheric~~ Climate index	Melt index	WS	IO	PO	RS	BAS	AIS	All
SAM	EMO	-0.27	0.77***	0.32	0.16	0.25	0.52*	0.31
	CMO	-0.03	0.15	0.03	0.50*	0.53*	0.80***	0.54**
	Melting days	0.37	0.18	0.01	-0.26	-0.42	-0.88***	-0.02
	MDF	0.18	-0.11	-0.07	-0.48*	-0.53*	-0.88***	-0.33
SOI	EMO	0.11	-0.08	-0.01	0.10	0.28	0.55**	0.19
	CMO	0.09	-0.23	0.14	-0.53*	-0.12	0.18	-0.31
	Melting days	0.03	-0.26	0.07	-0.11	0.46*	-0.03	-0.07
	MDF	-0.16	-0.18	0.12	0.15	0.34	-0.03	-0.09
Nino3.4	EMO	-0.28	-0.06	-0.11	-0.02	-0.26	-0.47*	-0.27
	CMO	-0.15	0.19	-0.35	0.66**	0.28	0.01	0.35
	Melting days	0.04	0.42	-0.16	0.08	-0.54**	-0.15	-0.07
	MDF	0.24	0.36	-0.11	-0.22	-0.46*	-0.15	0.13
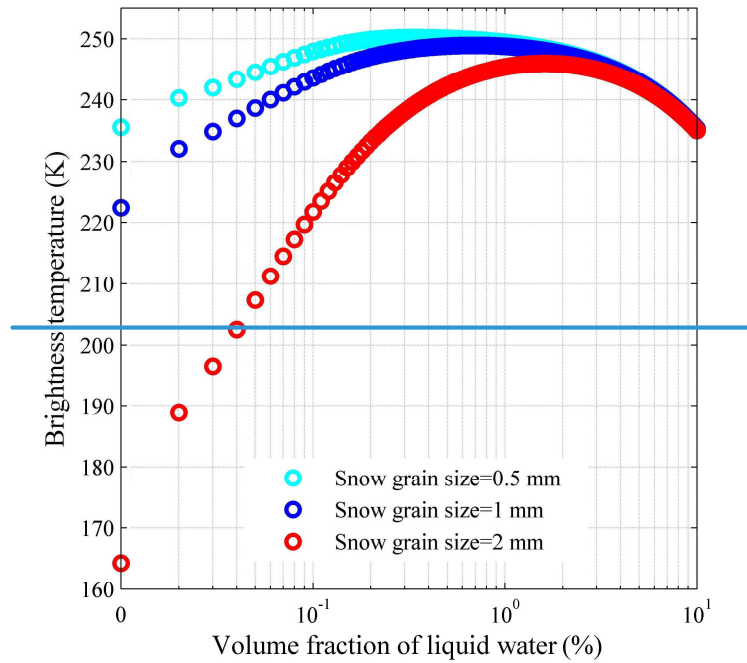
Figure 1. Simulated Tb$_{V36}$ varying with liquid water when the snow grain size is 0.5 cm (cyan), 1 mm (blue) and 2 mm (red).
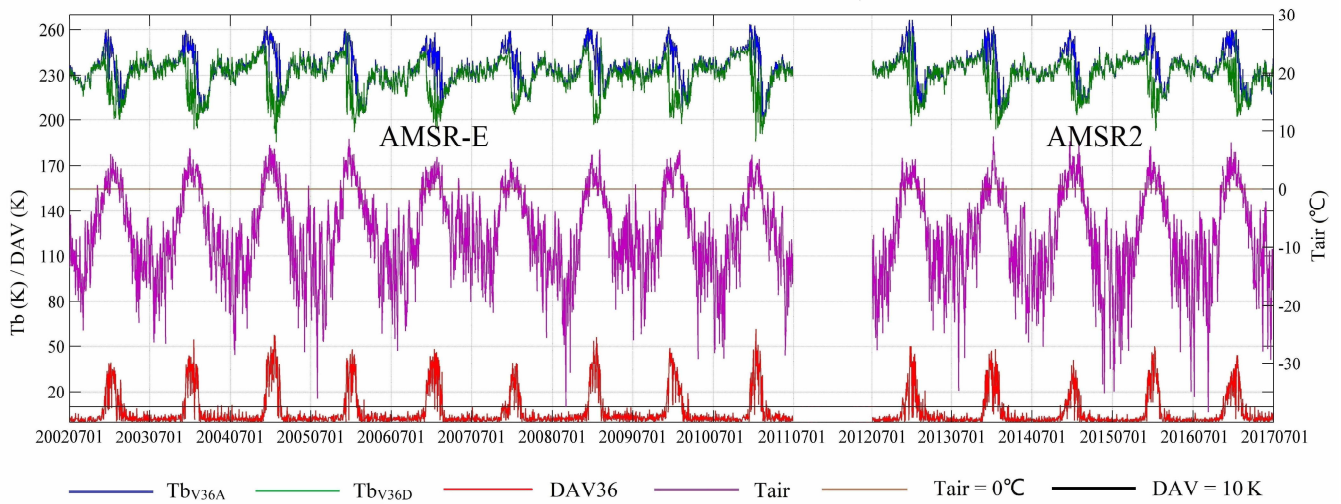
5 **Figure 2̶1. The comparison between Tair and satellite observations (AMSR-E from 2002 to 2011 and AMSR2 from 2012 to 2017) at Zhongshan Station, including daily maximum Tair (purple line), Tb$_{V36A}$ (dark blue line), Tb$_{V36D}$ (dark green line) and DAV36 (red line); Brown and black lines represent Tair = 0℃ and DAV = 10 K.**
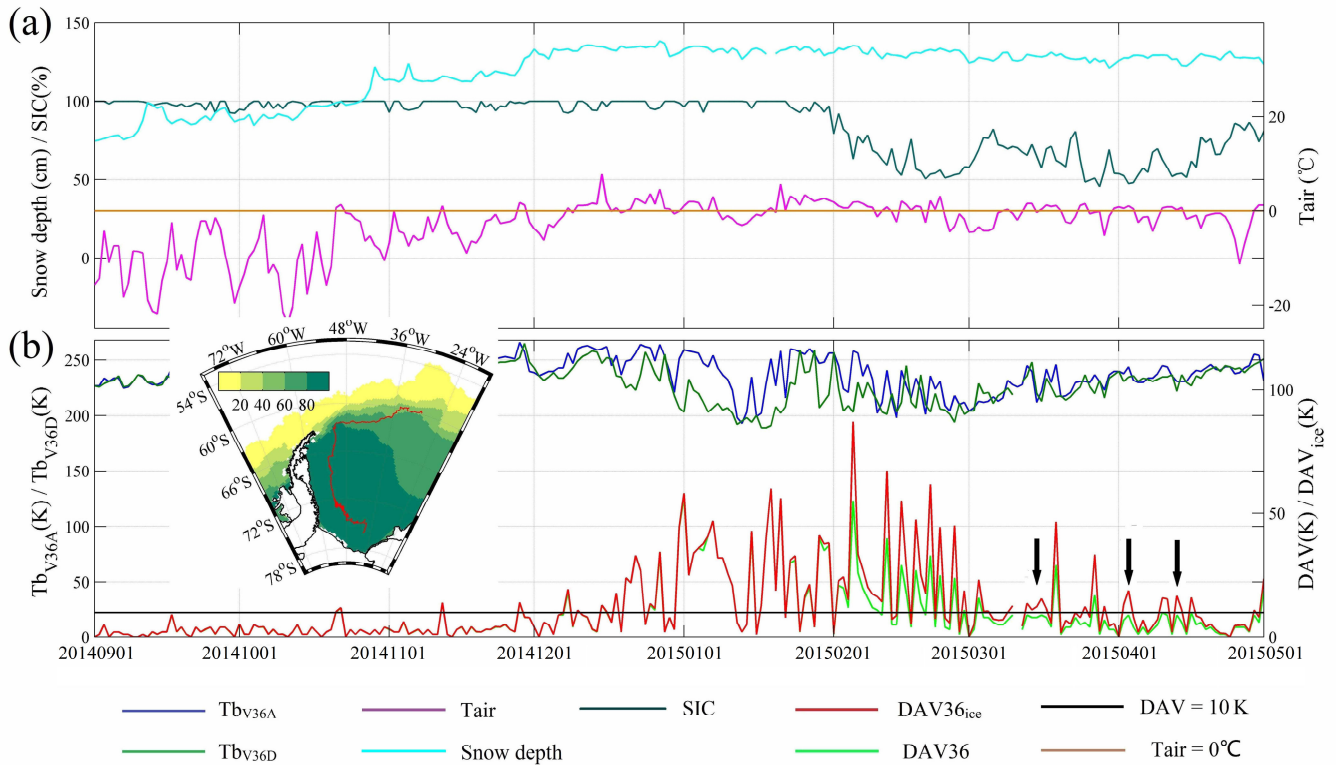
23

Figure 32. Meteorological and satellite measurements along a sea ice buoy in the Weddell Sea from 1 September, 2014 to 1 May, 2015. (a) Snow depth (cyan line), daily maximum Tair (pink line), and SIC (olive line); the brown line represents Tair = 0°C. (b) Tb_{V36A} (dark blue line), Tb_{V36D} (dark green line), DAV36 (light green line) and $DAV36_{ice}$ (red line); the black line represents DAV=10 K. The inset map in (b) illustrates the annual mean SIC and the route of the buoy from multi-year ice to first-year ice. The black arrows indicate the cases that melt events were recognized by $DAV36_{ice}$ rather than DAV36.
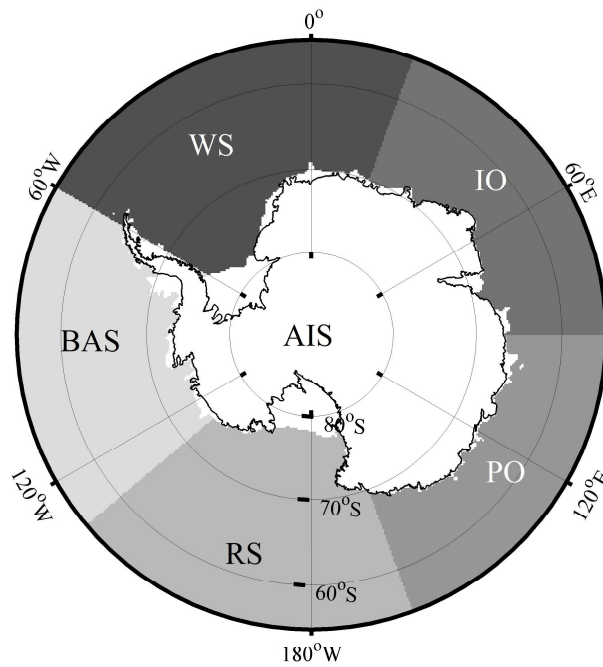
WS-*Weddell Sea*   **IO**-*Indian Ocean*   **PO**-*Pacific Ocean*   **RS**-*Ross Sea*

BAS-*Bellingshausen Amundsen Sea*   **AIS**-*Antarctic ice sheet*

Figure 43. Map of the different regions across the pan-Antarctic.

5

10

15

25
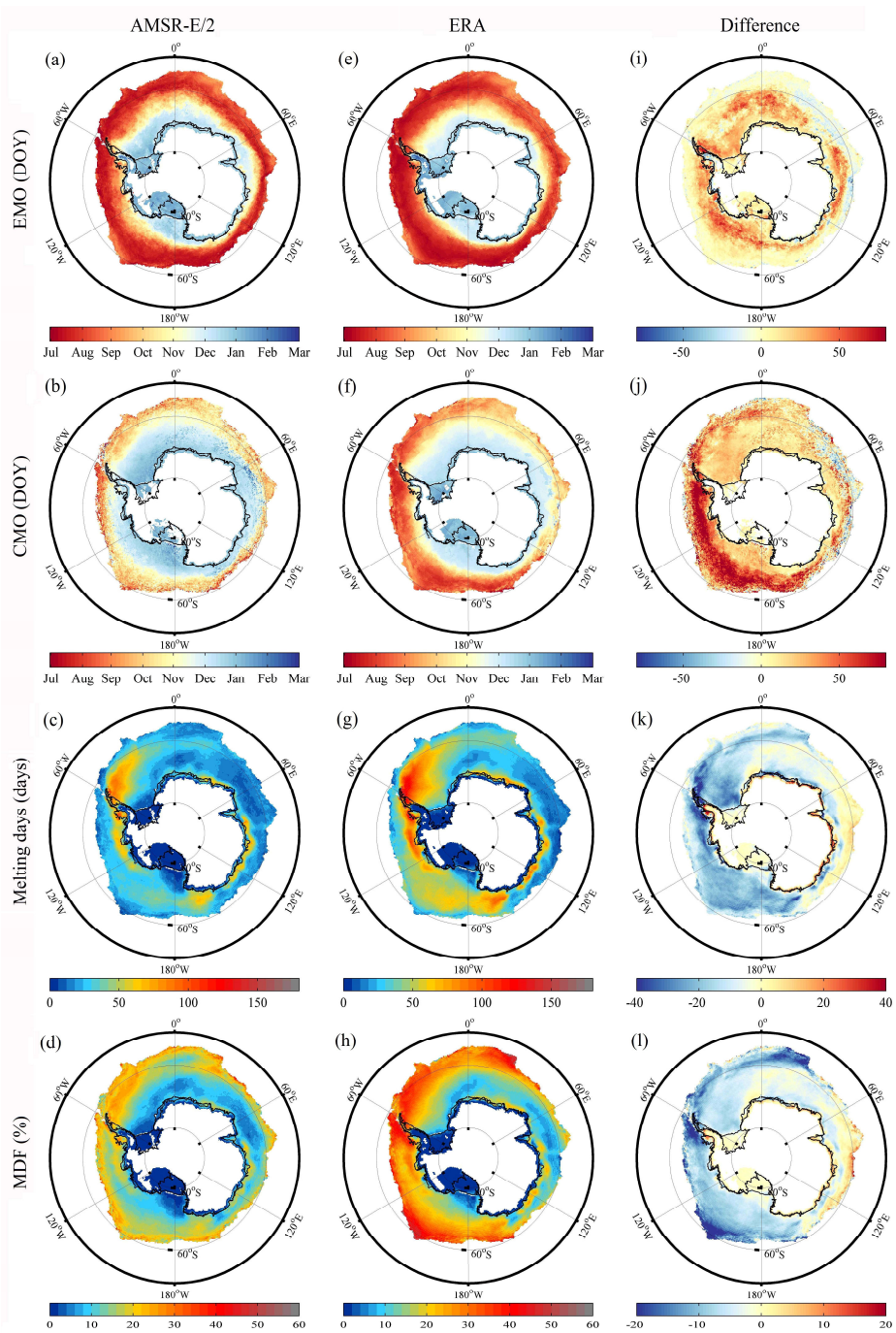
Figure 54. Annual mean EMO, CMO, melting days and MDF derived by AMSR-E/2 (a-d) and ERA-**Interim** (e-h), also shown are the differences (AMSR-E/2 minus ERA-**Interim**) between the two observations (i-l).
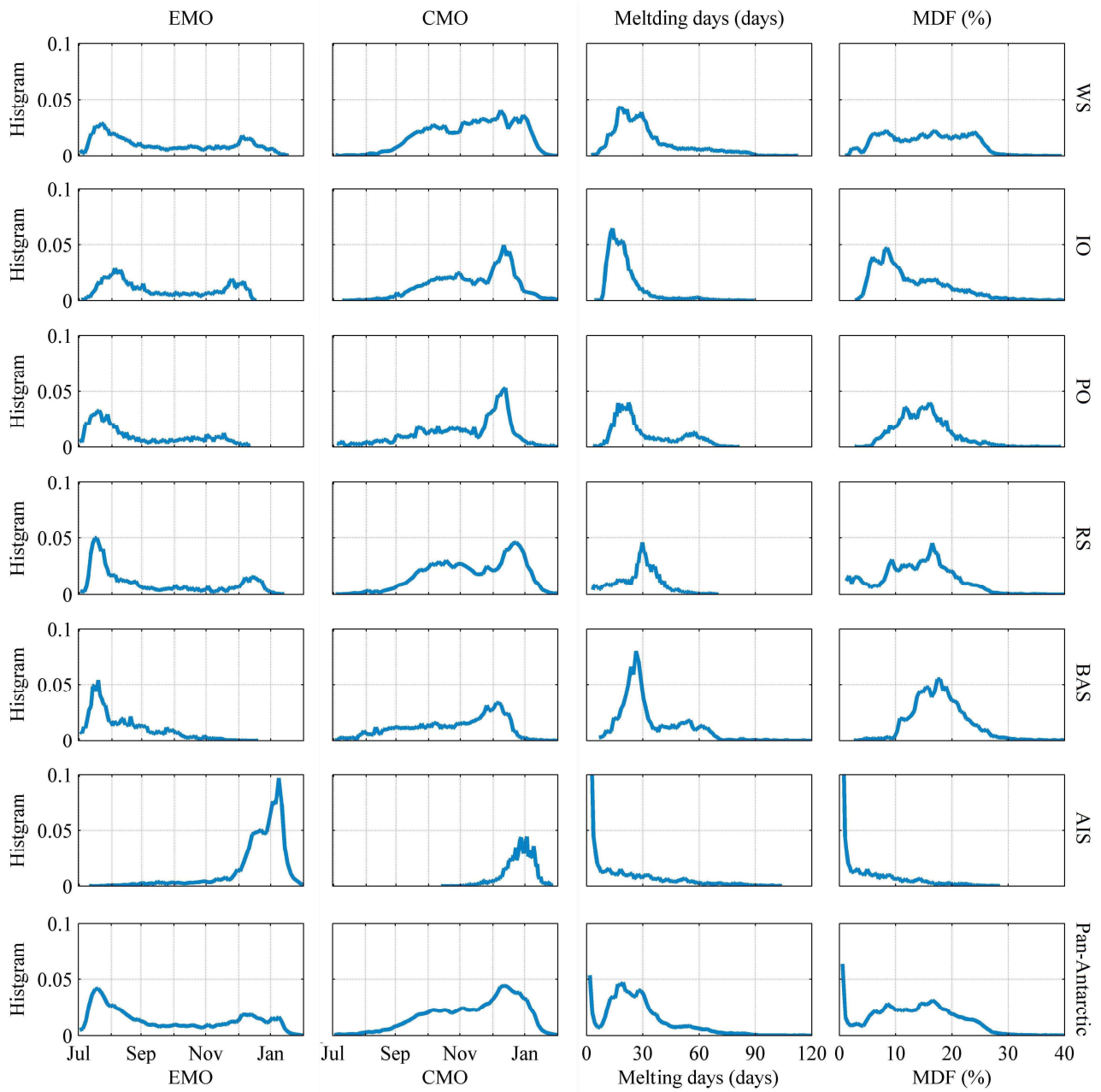
Figure 65. Normalized histograms of annual mean EMO, CMO, melting days and MDF for pan-Antarctic and different regions.

5
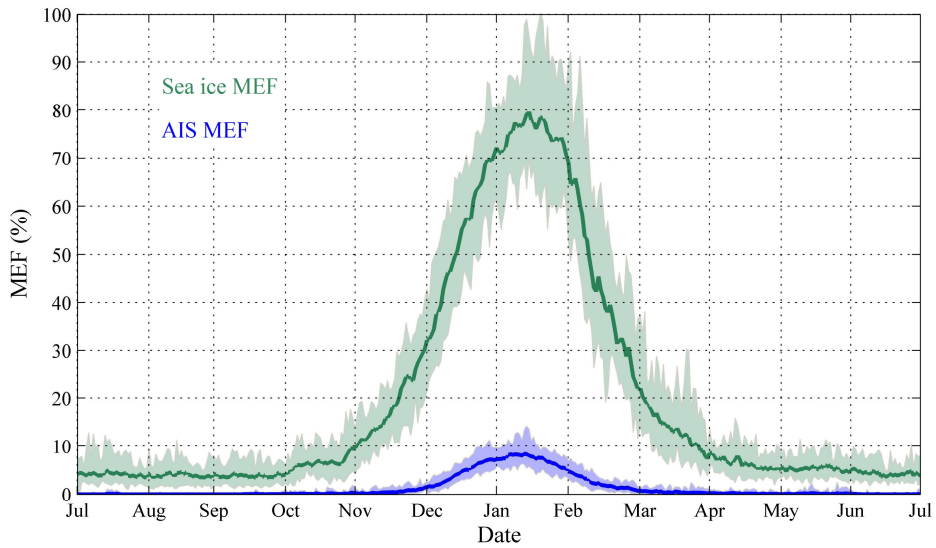
Figure ~~7~~6. Daily mean Antarctic sea ice MEF and AIS MEF, the corresponding shadows indicate daily maximums and minimums.
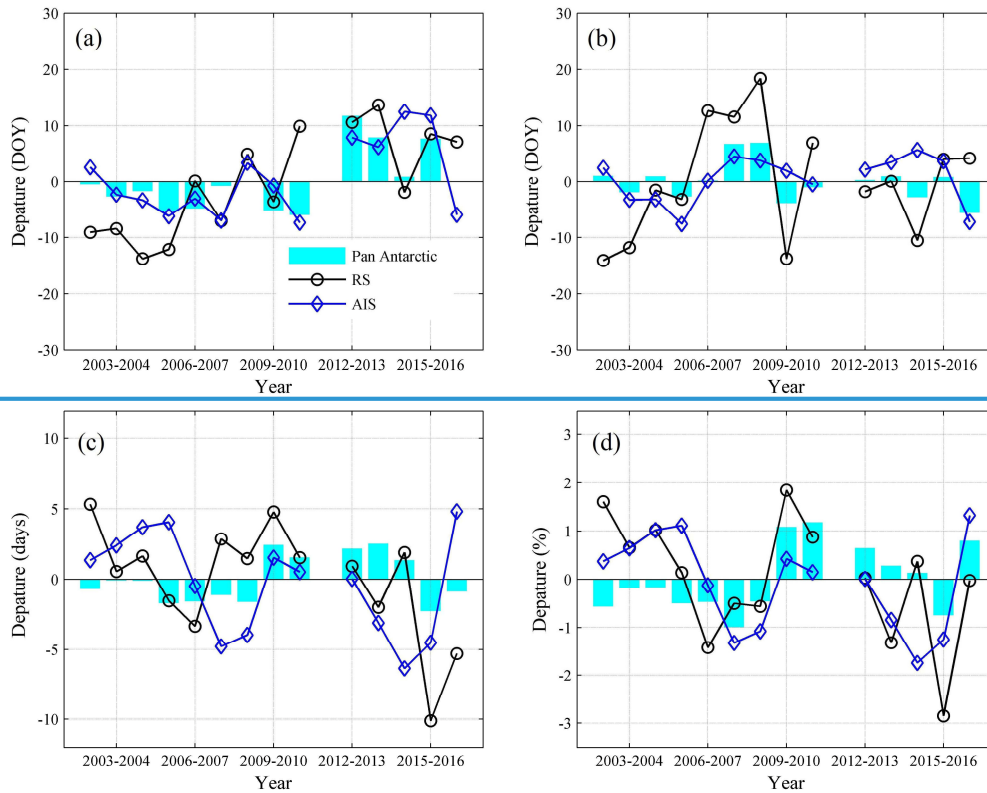
5

28
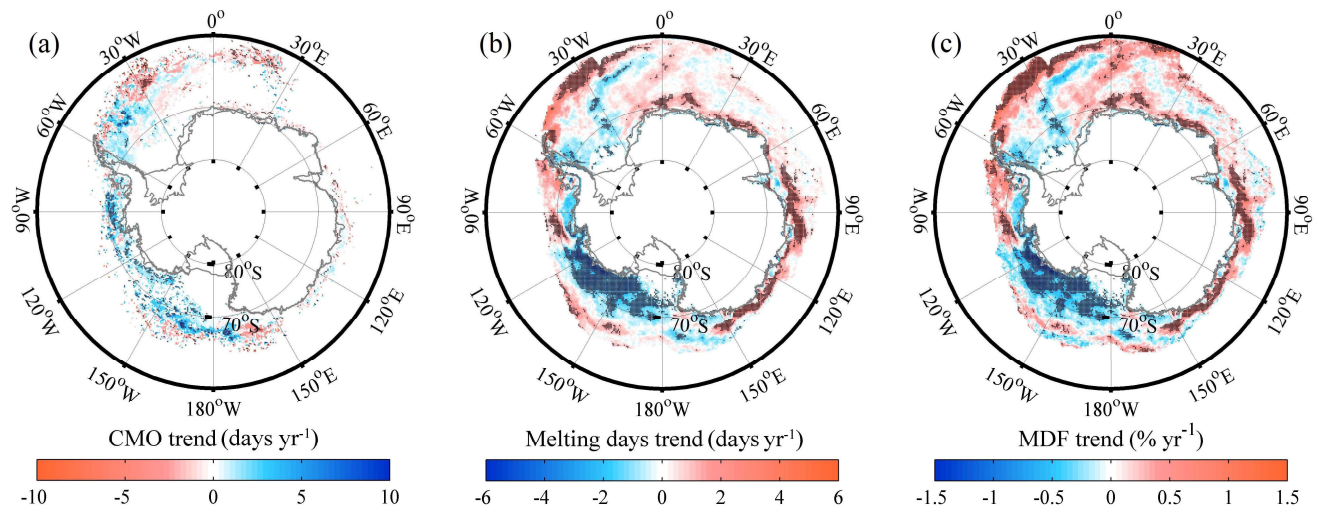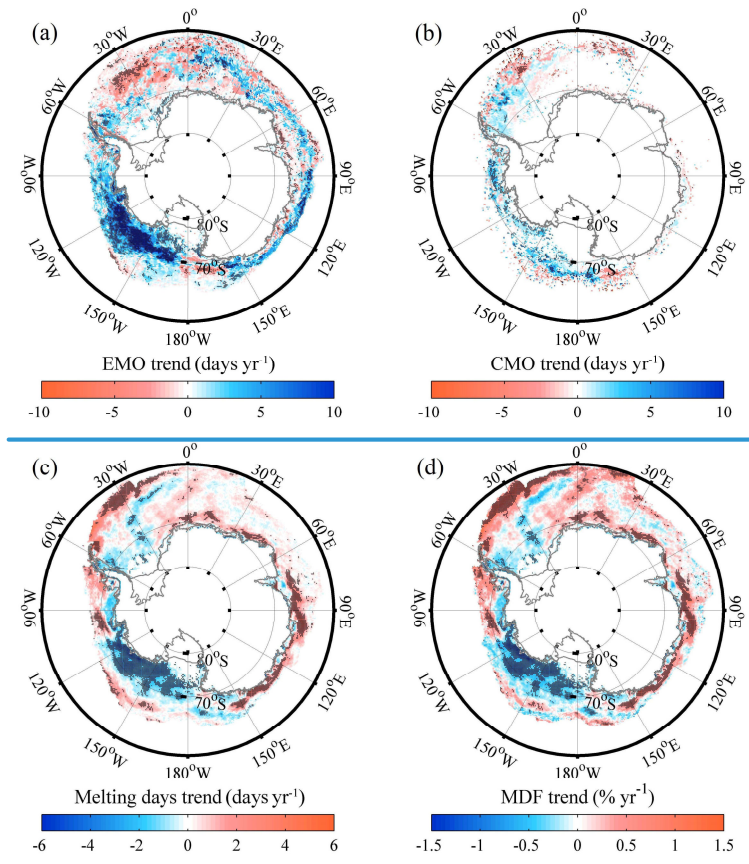
Figure 97. Trends in (a) ~~EMO (b)~~ CMO, (e_b) melting days and (d_c) MDF, black points indicate the pixels with trends above the 90% confidence level.
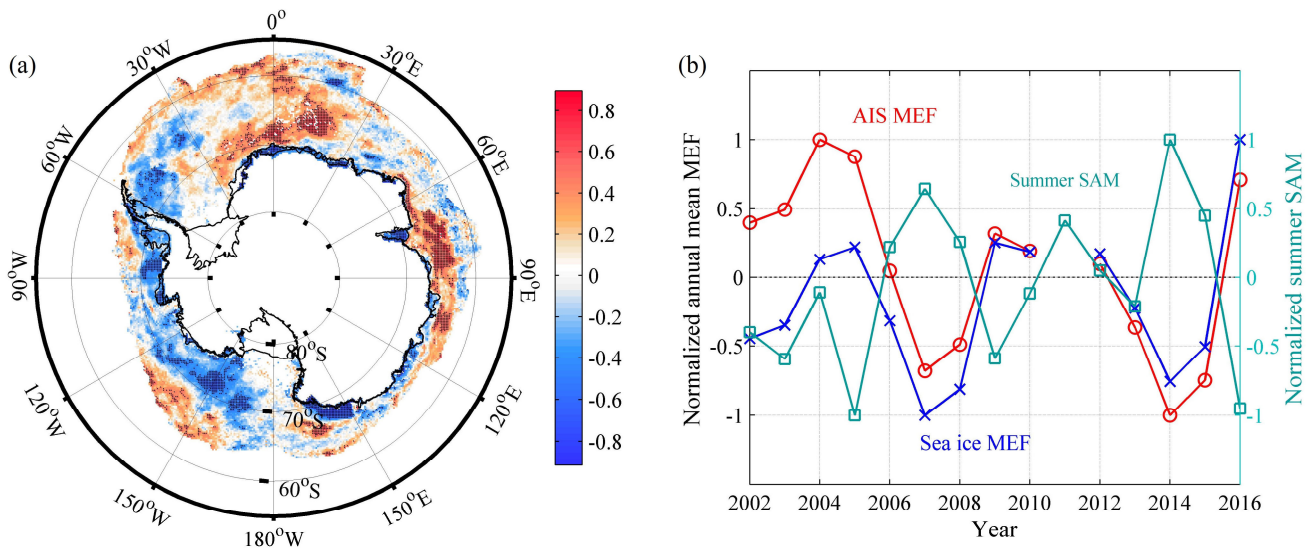
Figure 8. Linkage between pan-Antarctic snowmelt and summer SAM. (a) Correlation coefficient between MDF and summer SAM, black points indicate the trends above the 90% confidence level. (b) Comparison of normalized summer SAM (cyan line), normalized annual mean Antarctic sea ice MEF (blue line) and AIS MEF (red line).
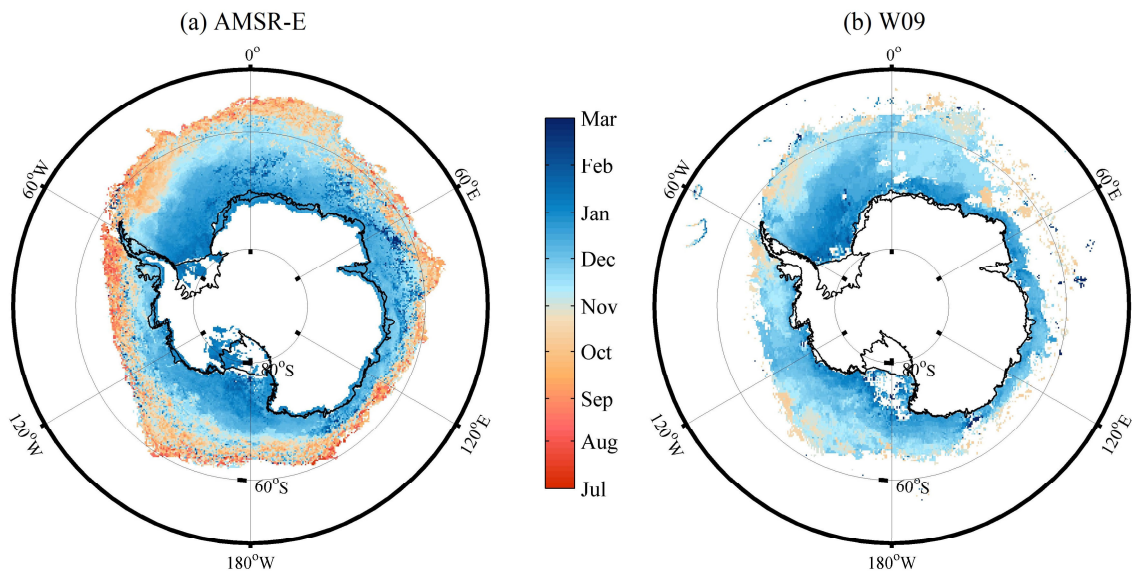
5

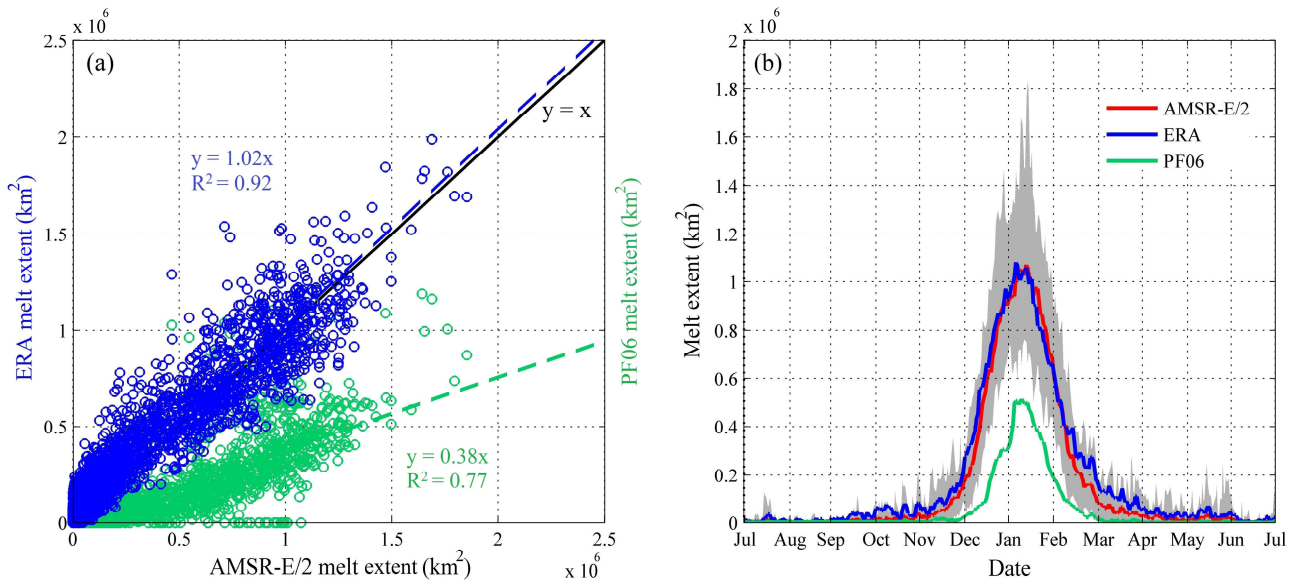**Figure ~~10~~9. Annual mean CMO derived from (a) AMSR-E and (b) W09 from 2002 to 2008.**

Figure ~~11~~10. Comparison of AIS melt extent derived by AMSR-E/2, ERA-Interim, and PF06 from 2002 to 2017. (a) Scatter plot of daily melt extent, blue circles indicate AMSR-E/2 vs. ERA-Interim and green circles indicate AMSR-E/2 vs. PF06. (b) Daily mean melt extent derived by AMSR-E/2 (red line), ERA-Interim (blue line) and PF06 (green line), grey shadow indicates the daily maximum and minimum melt extent detected by AMSR-E/2.
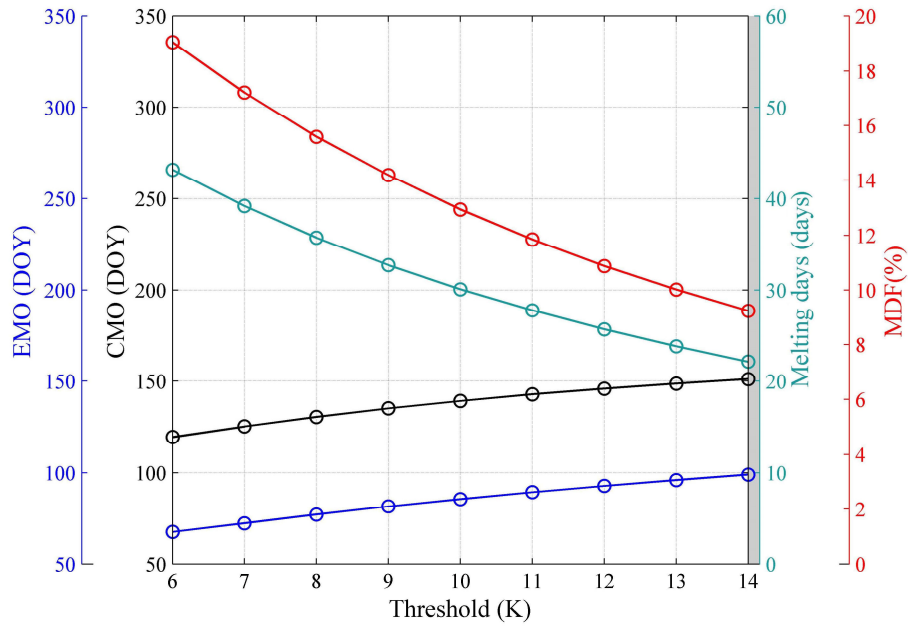
Figure ~~12~~11. Annual mean EMO (blue dots), CMO (black dots), melting days (cyan dots) and MDF (red dots) with the threshold for AMSR-E/2 DAV36 varying from 6-14 K.
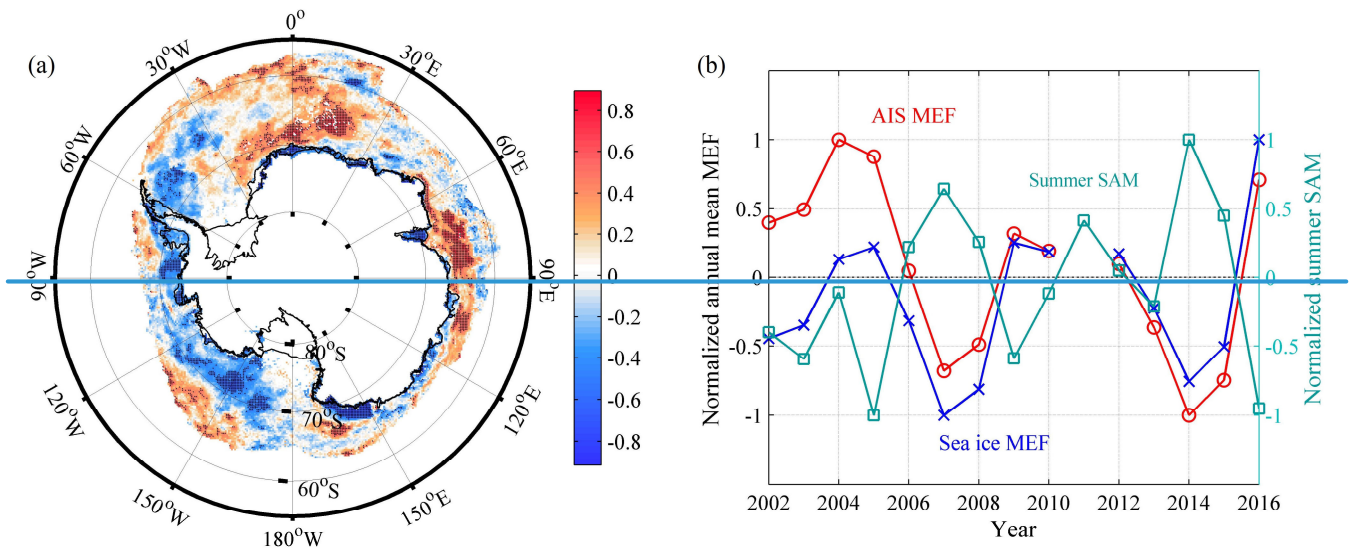

5   ~~Figure 13. Linkage between pan-Antarctic snowmelt and summer SAM. (a) Correlation coefficient between MDF and summer SAM, black points indicate the trends above 90% confidence level. (b) Comparison of normalized summer SAM (cyan line), normalized annual mean Antarctic sea ice MEF (blue line) and AIS MEF (red line).~~